NASA TECHNICAL REPORT

NASA TR R-207




NASA TR R-207

# MASS ADDITION IN THE STAGNATION REGION FOR VELOCITY UP TO 50,000 FEET PER SECOND

*by John T. Howe and Yvonne S. Sheaffer*

*Ames Research Center*
*Moffett Field, Calif.*

NATIONAL AERONAUTICS AND SPACE ADMINISTRATION • WASHINGTON, D. C. • AUGUST 1964

# MASS ADDITION IN THE STAGNATION REGION FOR VELOCITY UP TO 50,000 FEET PER SECOND

By John T. Howe and Yvonne S. Sheaffer

Ames Research Center
Moffett Field, Calif.

NATIONAL AERONAUTICS AND SPACE ADMINISTRATION

For sale by the Office of Technical Services, Department of Commerce,
Washington, D.C. 20230 -- Price $1.50

# MASS ADDITION IN THE STAGNATION REGION FOR VELOCITY UP TO 50,000 FEET PER SECOND

By John T. Howe and Yvonne S. Sheaffer

Ames Research Center
Moffett Field, Calif.

## SUMMARY

Solutions of the viscous shock layer equations with mass addition are obtained. Flow-field equations include the effects of heat conduction, diffusion of reacting species, and emission and absorption of gaseous radiation for dissociated and partially ionized air in chemical equilibrium. Convective and radiative heating rates with mass addition are obtained from the solutions. Algebraic equations are derived for predicting the nose radius that minimizes total heating rates at a given flight speed and shock-layer pressure level. Values for the corresponding natural ablation rate, the effective heat of ablation, the ratio of radiative to convective heating rate, surface shear stress, and shock-wave standoff distance are given. The effects of ablated gases that radiate more strongly than air are examined. Rules for scaling flow-field structure with mass addition are discussed. Solutions without mass addition at low Reynolds numbers where external vorticity, energy depletion, and flow energy limiting are important are compared with existing theory and experiments.

## INTRODUCTION

The study of mass addition in the stagnation region is of interest because any object, blunt or pointed, which enters the atmosphere at high speed will generally have a blunted stagnation region as the material suffers thermal erosion. Interest is further enhanced because the aerodynamic heating rate is likely to be a maximum in the stagnation region.

The hot thin gas cap over the forward surface of an object entering a planetary atmosphere is the host to a myriad of interrelated physical phenomena. The study of the gas cap is especially cumbersome if the flow field is a mixture of air and foreign species which were added to the flow because the surface is ablating. The knowledge of mass addition effects at speeds below which ionization and gaseous radiation effects may be neglected is very highly developed from both the flow field and materials points of view. (A small part of the extensive literature on the subject will be brought into the discussion subsequently where appropriate.) On the other hand, mass addition at speeds greater than 30,000 ft/sec for which the gas cap is both ionized and radiating has received comparatively little attention.

The purpose of this paper is to examine the effects of mass addition at flight speeds greater than 30,000 ft/sec as it influences and is influenced by some of the many other phenomena, parameters, and physical properties of the gas cap. To this end we consider mass addition in the general sense, transpiration, and in the special sense, ablation.

For mass addition in general, we particularly want to know its influence on convective heating. Is heat blockage as effective at the higher speeds as it is at the lower speeds? Do the existing correlation formulas obtained for lower speeds apply at high speeds?

With respect to ablation, we are especially interested in finding the conditions for which the total heating rate at a given flight condition and given material is minimized, for two reasons. First, minimum heating of itself is intrinsically advantageous. Second, it gives one ideal situation in terms of nose radius and ablation rate at each flight condition for which we can examine some of the other questions of interest, thus affording some economy in the range in which other parameters need be varied. We obtain an appreciation of what may be achieved under advantageous conditions.

Other questions have to do with the effect of mass addition on related quantities. For example, we may expect that mass addition will alter the flow-field structure and change the standoff distance. At once the question arises, What is the effect of altered standoff distance on radiative heating? Moreover, the species added to the flow field may be expected to radiate differently from air. The question is, How important might this effect be? Some ablating materials suffer from lack of physical strength, so we are interested in the magnitude of viscous shear stresses at the surface and how they compare with pressure stresses. We are, of course, concerned with the relative importance of radiative to convective heating because it bears on the type of surface useful for heat shielding, and it indicates where improvements in our knowledge are more important - in gaseous radiation emission properties or in total thermal conductivity of the gas. Ablation rates and effective heat of ablation are of course important to determine at speeds greater than 30,000 ft/sec.

Because much of the experimental work on mass addition is performed in ground-based facilities for which both the entry object and the environment must be modeled, we wish to examine the problem of scaling mass addition effects.

Finally, because of increasing interest in pointed or very slightly blunted entry bodies, low Reynolds number (based on nose radius) effects or external vorticity effects have become important. This problem will be examined briefly.

## SYMBOLS

| | |
|---|---|
| $A$ | defined by equation (13) |
| $a$ | asymptote in expression for $\psi$ |
| $B$ | defined by equation (10) |
| $b$ | exponent in equation (2), evaluated in equations (3) and (4) |
| $C$ | defined by equation (13) |
| $C_H$ | ratio of convective heat-transfer rate to free-stream energy flux |
| $c_f$ | local mass fraction of inert foreign species f or "pseudo" mass fraction of reacting foreign species f (ref. 2) |
| $c_i$ | local mass fraction of species i of ablation products |
| $c_{p_i}$ | specific heat at constant pressure for species i |
| $D$ | defined by equation (13) |
| $D_f$ | diffusion coefficient of species f |
| $E_n$ | defined by equation (A12) |
| $f$ | dimensionless stream function defined by equation (A20) |
| $f_w$ | dimensionless stream function at the wall |
| $g$ | dimensionless enthalpy defined by equation (A22) |
| $H$ | defined by equation (A2) |
| $h$ | static enthalpy, equation (A9) |
| $h_a$ | intrinsic heat of ablation defined by equation (6) |
| $h_{eff}$ | effective heat of ablation defined by equation (16) |
| $h_{i_v}$ | heat of vaporization of species i |
| $j$ | total enthalpy, equation (A8) |
| $K$ | Planck mean mass absorption coefficient |
| $\overline{K}$ | dimensionless coefficient, $\frac{K}{K_s}$ |
| $k$ | zero for two-dimensional flow; unity for axisymmetric flow |

| | |
|---|---|
| $\dot{m}$ | surface mass loss rate per unit area defined by equation (1) |
| n | exponent in equation (2), usually 3/2 |
| Pr | equivalent Prandtl number containing actual specific heat of mixture and total thermal conductivity |
| p | static pressure |
| $q_c$ | convective heating flux at the surface with blowing |
| $q_{c_o}$ | convective heating flux without blowing |
| $q_r$ | net radiative heating flux accepted by the wall with blowing; defined by equation (9) |
| $q_{r_o}$ | net radiative heating flux accepted by the wall without blowing |
| $q_{r_g}$ | incident gaseous radiant flux accepted by the wall with blowing |
| $q_T$ | net heating flux accepted by the wall with blowing, equation (5) |
| $q_{T_o}$ | net heating flux accepted by the wall without blowing |
| R | body nose radius |
| R* | optimum nose radius which minimizes total heating |
| Re | Reynolds number, $\frac{\rho_\infty UR}{\mu_s}$, except for figures 28, 29, 30 where it is defined by the abscissa |
| r | defined by sketch (a) |
| Sc | Schmidt number, $\frac{\mu}{\rho D_f}$ |
| T | absolute temperature |
| $\overline{T}$ | dimensionless temperature, $\frac{T}{T_s}$ |
| t | dummy optical depth |
| U | flight velocity |
| $\overline{U}$ | dimensionless flight velocity $U(ft/sec)/10^4(ft/sec)$ |
| u | velocity parallel to body surface |
| $\vec{V}_i$ | total velocity of species i (mass average + diffusion velocity) |
| v | velocity normal to body surface |

| | |
|---|---|
| $x$ | distance from stagnation point along body surface |
| $y$ | distance normal to body surface |
| $\alpha$ | approximate ratio of absorption coefficient of foreign gas to that of air at shock-layer pressure level and wall temperature (ref. 1, p. 6) |
| $\alpha_w$ | fraction of incident gaseous radiation accepted by wall; sum of surface absorptivity and transmissivity |
| $\beta$ | constant in equation (22); depends on wall material |
| $\delta$ | shock-wave standoff distance |
| $\epsilon$ | density ratio across shock wave, $\frac{\rho_\infty}{\rho_s}$ |
| $\epsilon_w$ | wall emissivity |
| $\eta$ | similarity variable defined by equation (A19) |
| $\mu$ | coefficient of viscosity |
| $\zeta$ | transformed coordinate parallel to the body surface defined by equation (A18) |
| $\rho$ | mass density |
| $\sigma$ | Stefan-Boltzmann constant |
| $\tau$ | optical depth defined by equation (A11) |
| $\tau_w$ | wall shear stress at body surface |
| $\varphi$ | defined by equation (A25) |
| $\psi$ | ratio of convective heating rate with to that without mass addition; $\frac{q_c}{q_{c_o}}$ |
| $\omega$ | stream function defined by equation (A17) |

Superscripts

| | |
|---|---|
| $'$, $''$, $'''$ | derivatives with respect to the independent variable |

## Subscripts

| | |
|---|---|
| a | refers to intrinsic heat of ablation |
| air | properties of air |
| c | convective |
| eff | effective |
| f | foreign species |
| g | gas |
| i | species i of ablation products |
| no vort | without vorticity in the flow external to the boundary layer |
| o | without blowing or ablation |
| r | radiative |
| s | conditions just behind the bow shock |
| T | total |
| v | vaporization |
| w | conditions at the wall |
| $\infty$ | free-stream conditions |

## GENERAL FEATURES OF SOLUTIONS

In this study, we are concerned with both the structure of the stagnation region flow field (which will be obtained from solutions of the flow-field equations), and with quantities derived from flow-field solutions. The details of the method of solution of the flow-field equations are contained in appendix A and in reference 1.

Briefly, the conservation equations for mass, momentum, and energy are solved in the stagnation region of blunt bodies from the body surface to the shock wave. Momentum transport by viscosity and energy transport by conduction, diffusion of reacting species, and emission and absorption of radiation are included in the integro-differential equations.

The thermodynamic and transport properties (radiative transport sometimes excepted as discussed subsequently) of the mixture of air and injected gases are assumed to be those of partially dissociated and ionized air in chemical equilibrium (ref. 1). This assumption should lead to reasonable results even if the injected gases become ionized, if the ablation products are nitrogen, oxygen, and carbon compounds, the reason being the similarities among these species and their compounds. That is the atomic weights of monatomic species are nearly alike, as are the molecular weights of diatomic species. Moreover, the dissociation energy of $CO_2$ is close to that of $O_2$; that of CN like that of NO, CO like $N_2$, while CO, N, and O all have nearly the same first ionization potential (which is not radically different from that of C). Actually, the

bulk of the injected species will be near the wall of the body where the temperature and degree of ionization are suppressed, and the argument of Lees (refs. 2 and 3) may be employed. For nonionized gas mixtures, Lees has shown that it is not necessary to understand the extraordinarily complicated details of the chemical interaction between the atmospheric gas components and the vaporized surface material insofar as convective energy transport is concerned as long as the molecular weights and collision cross sections of the injected gas and air are of comparable size, or that the ratio of mass diffusivity to thermal diffusivity (Lewis number) of the mixture be near unity.

On the other hand, radiative transport by the mixture of injected vapor and air may be significantly different from that of air alone. This behavior is allowed for in the governing equations by including a quantity proportional to the injected species concentration in the Planck mean mass absorption coefficient expression and a diffusion equation to account for this species. In the results to be presented, radiation from injected gases is specified to be like that of air except where stated to the contrary.

The results of the analysis have been tested against those by others where possible in order to establish the validity of the method. In reference 1 it was shown that the calculated structure of the flow field exhibits both an isoenergetic shock layer and a boundary layer in the low speed (such that energy depletion by radiation is negligible) high Reynolds number regime as it should. The analysis reproduced the well-known effects on convective heating of the assumption $\rho\mu$ = const when $\rho\mu$ was artificially set constant. The shock standoff distances predicted by this method agree with those predicted by other methods (e.g., ref. 4). When radiation coupling is negligible, it produces convective heating results at high speeds (up to 50,000 ft/sec) that agree with the boundary-layer results of references 5 and 6 which use the same transport properties. It will be seen subsequently that in the low Reynolds number regime the method leads to flow fields which exhibit the expected shock-layer vorticity structure and the corresponding enhanced surface shear stress and convective heating rates. One additional test of the method is shown in figure 1. The solid lines are enthalpy profiles across the flow field for the nose radii and flight conditions noted, and the symbols are the results of K. K. Yoshikawa (ref. 7), corresponding to the one-dimensional flow of radiating air behind the shock wave. It is seen that both analyses show that the shock layer is nonisoenergetic and both give the same results for that half of the flow field nearest the shock. The present analysis, of course, shows lower enthalpy and larger enthalpy gradients as a result of convective transport in that half of the flow field near the body because neither a body nor energy transport by conduction was included in the one-dimensional analysis of reference 7.

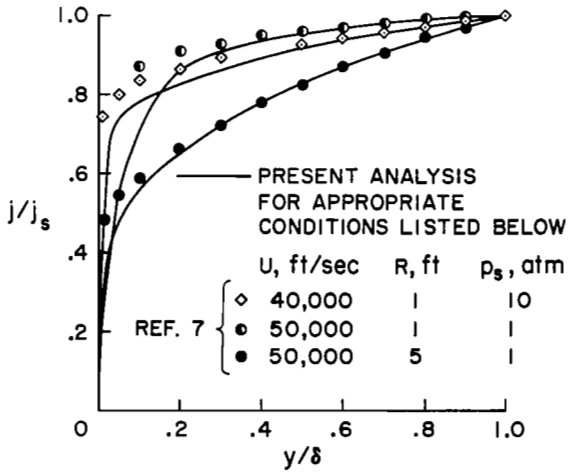


Figure 1.- Comparison of enthalpy profiles with those of reference 7.

Before mass addition effects are discussed, a brief comment should be made regarding terminology. Throughout the rest of the paper, comments relating to mass addition and injected gases, in general, apply to both forced mass addition (transpiration) and natural mass addition (thermal erosion or ablation). When our comments are specialized to thermal erosion only, the word ablation will be used.

## EFFECTS OF MASS ADDITION ON HEATING RATES

### Radiative Heating

Mass addition can affect radiative heating in two ways; by altering the temperature and structure of the flow field and by adding species which radiate differently from air. However, results of numerous flow-field solutions[1] with mass addition show that (except for a combination of low Reynolds number and strong injection of gases which radiate more strongly than air, discussed subsequently) radiative heating is much less affected by mass addition than is convective heating.

Mass addition of gases like air tends to thicken the shock layer thus tending to enhance radiative heating, but it also tends to cool the flow field - inhibiting radiative heating. In almost all of the solutions the net effect of injection of a species which radiates like air was to increase radiative heating modestly. For example, for a flight speed of 50,000 ft/sec, a nose radius of 0.25 foot, a shock-layer pressure level of 1 atmosphere, and a surface mass flux of 13 percent of the free-stream mass flux ($f_w = -1.5$), the radiative heating was enhanced about 24 percent.

Moreover, it was shown in figure 9 of reference 1 that for high Reynolds number, the bulk of the injected species remains close to the vehicle surface where the temperature is low compared with that behind the shock wave. Thus the radiant flux at the surface is enhanced only 7 percent by a gas which emits 50 times as strongly as air injected at the same rate ($f_w = -0.4$, or mass addition rate 2 percent of the free-stream mass flux; same flight condition as above with $R = 1$ ft).

On the other hand, it will be shown subsequently (in the discussion of fig. 18) that if the Reynolds number is low, injected species will also be present in the hot part of the flow field and need not radiate much more strongly than air in order to have an appreciable effect on radiative heating.

---

[1]All of the results of this section of the paper correspond to wall temperatures between 1500° and 3000° K.

## Convective Heating

Convective heating is, of course, very strongly influenced by mass addition. In the flight regime for which air is dissociated but not ionized, many studies (see Adams, ref. 8) have employed a linear approximation relating $\psi$ (the ratio of convective heating with mass addition to that without) to the product of mass addition rate and driving enthalpy divided by the convective heating without mass addition. The linear $\psi$ was based upon an empirical correlation of experimental and theoretical transpiration results from references 9, 10, and 11. Swann (ref. 12) and Swann and Pittman (ref. 13) obtained a quadratic expression for $\psi$ in terms of the above variables by an empirical fit of the results of ideal gas boundary-layer solutions of Beckwith (ref. 14).

In the present analysis, the influence of mass addition on convective heating was obtained from results of the ionized radiating flow-field solutions (both $q_c$ and $q_{c_o}$ were obtained from the solutions). The parameter $\psi$ for speeds of 40,000 and 50,000 ft/sec is shown in figure 2 as a function of $f_w$, the dimensionless stream function at the wall. The quantity $f_w$ is proportional to the mass addition rate by the relation

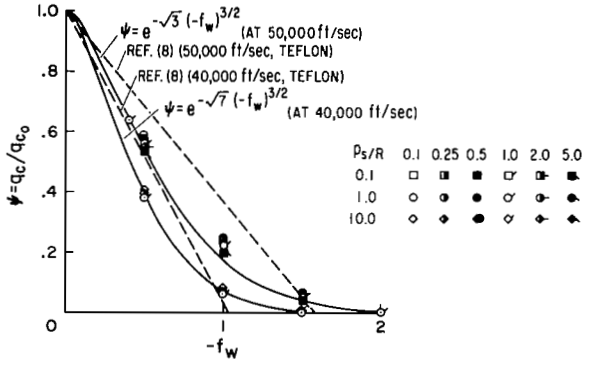


Figure 2.- Separate correlations of results of blowing on convection at U = 40,000 and 50,000 ft/sec.

$$\dot{m} = \rho_w v_w = -f_w \sqrt{\frac{\rho_s \mu_s U(k+1)}{R}} \tag{1}$$

For the moment, attention is directed to the solid curves of the figure. (The dashed lines are an application of the linear $\psi$ approximation and will be discussed in a subsequent section of the paper.) Each solid line correlates results for one flight speed, various nose radii, and various shock-layer pressure levels as can be seen from a comparison with the plotted symbols. Each of these curves is represented by the exponential

$$\psi = e^{-b(-f_w)^n} \qquad (2)^2$$

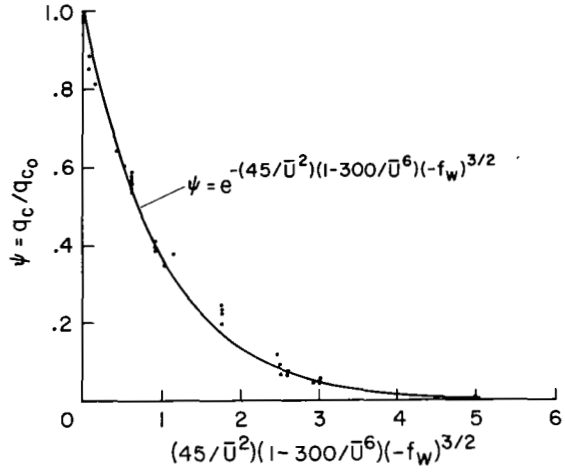


Figure 3.- General correlation of result of blowing on convection. (The points are identified in table I.)

where b is a function of flight velocity alone and n is 3/2. Similar curves can be constructed for other flight velocities. Note that a given $f_w$ is less effective in retarding convective heating at higher speeds.

We can correlate results over a wide range of conditions by expressing b as a function of U. That is, results of 36 mass addition solutions for nose radii[3] ranging from 0.01 to 5 feet, flight speeds from 30,000 to 50,000 ft/sec, and shock-layer pressure levels from 0.1 to 10 atmospheres are correlated in figure 3 by use of equation (2) with

$$b = \frac{45}{\bar{U}^2}\left(1 - \frac{300}{\bar{U}^6}\right) \qquad (3)$$

---

[2]Some experiments by Vojvodich, Pope, and Dickey of Ames Research Center at conditions corresponding to subsatellite speed indicate that $\psi$ for strong ablation of some materials may approach an asymptote different from zero; possibly of the order of $10^{-1}$ (this effect was remarked upon in ref. 15). An appropriate form of $\psi$ for that case would be $\psi = a + (1 - a)e^{-b(-f_w)^n}$ where a is the value of the asymptote. The asymptote does not appear to be caused by wall temperature effects alone. In the examples of figures 2 and 3, no asymptote other than zero could be distinguished even though wall temperature was changed from 1500° to 3000° K. For example, at 40,000 ft/sec flight speed, 1 atmosphere shock-layer pressure level, 1-foot nose radius, and $f_w = -1.0$, both $q_c$ and $q_{c_o}$ changed as $T_w$ was changed from 1500° to 3000° K, but their ratio $\psi$ remained the same to four decimal places, 0.0626. It is conceivable that molecular weight of surface vapors may have something to do with the asymptote. For example, the vaporization temperature of Teflon is low enough that surface vapors may have a molecular weight of 100 rather than that between 16 and 30 for the air injection (or for that matter, 15 for vaporizing phenolic nylon) under consideration. This large a disparity in molecular weight may be significant and would tend to raise $\psi$ for the higher molecular weight gas. The presence of an asymptote different from zero would have important consequences from the practical point of view. Ablation materials should be sought which do not have a finite asymptote.

[3]Two points should be mentioned in connection with the small nose radii. First, the correlation holds for examples for which there is strong vorticity in the entire flow field as long as $q_{c_o}$ also includes the external vorticity effect. Secondly, the chemical equilibrium assumption is somewhat in doubt for the small nose radii, a point which will be discussed subsequently.

and $n = 3/2$. This formula is useful for extrapolation to flight speeds above 50,000 ft/sec, but cannot be used for speeds much below 30,000 ft/sec because it changes sign at about 26,000 ft/sec. The same mass addition solution results are correlated by letting:

$$b = 0.706 + 1.6\bar{U} - 0.28\bar{U}^2 \qquad (4)$$

and $n = 3/2$. The result is shown in figure 4. This formula can be used to extrapolate to speeds below 30,000 ft/sec, but cannot be used for speeds much above 50,000 ft/sec, because it changes sign at about 61,000 ft/sec.

The flight condition, nose radius, and value of $f_w$ for each point shown in figures 3 and 4 are listed in table I. Groups of points are numbered consecutively from left to right on the figure. Points within a group are numbered consecutively from top to bottom.

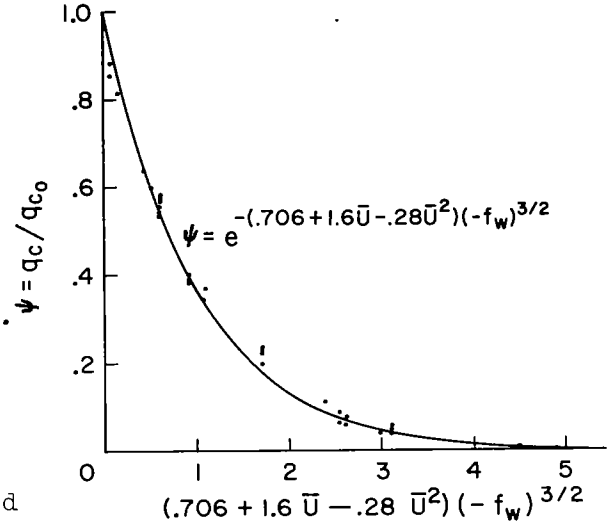


Figure 4.- General correlation of result of blowing on convection. (The points are identified in table I.)

These same results are also compared in figure 5 with the linear $\psi$ approximation of reference 8 and quadratic $\psi$ approximation of reference 13. The points on the figure correspond to our solutions listed in table II, where now the points are simply numbered from left to right in figure 5. In the figure, if the constant 0.49 in the linear approximation corresponding to Teflon (which would be 0.5 for phenolic nylon (ref. 8)) is changed to 0.6 (mentioned by ref. 8 as obtained from refs. 9, 10, 11), the fit is improved for the initial part of the data out to about $j_s\dot{m}/(-q_{c_o})$ equal to unity. Clearly, however, it cannot be made to fit the results beyond unity.

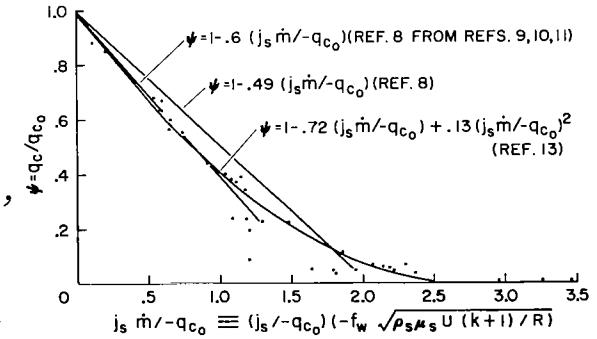


Figure 5.- Present results compared with other correlation formulas. (The points are identified in table II.)

The quadratic expression of reference 13 fits the present result well for $j_s\dot{m}/(-q_{c_o})$ equal to unity also, but not beyond. That approximation is set to zero when $j_s\dot{m}/(-q_{c_o})$ is 2.5. However, three points are shown to the right of 2.5 for which $\psi \neq 0$. Subsequently, during the examination of special conditions which minimize total heating rate, it will be important to have a simple correlation which must differ from zero at the high mass addition rates, for if $\psi$ were zero, the radius which minimizes total heating would be that which minimizes radiative heating, namely, zero. The exponential correlation (eq. (2)) will be especially useful in that regard.

The two approximations were obtained from relatively low speed results for which the air was either dissociated or inert, and it is not surprising to see that they do not fit the present results which include (among other differences) thermodynamic and transport properties of partially ionized air and are extended to higher values of $j_s\dot{m}/(-q_{co})$.

The simple expression (2) describing the effects of mass addition on convective heating at high speeds can now be applied with other information to the special case of mass addition by ablation.

## ABLATION

### General Relations for Ablation Quantities

Subliming ablators are attractive for heat protection because of heat absorption due to vaporization and the heat blockage effect in the boundary layer. Moreover, high-temperature subliming ablators have still another asset - the rejection of heat by reradiation.

On the other hand, at conditions corresponding to subsatellite speeds, subliming ablators have at least one liability from the heat rejection point of view. A theoretical study of Scala (ref. 16) shows that reactions between air and a graphite surface impose a significant heat load on the vehicle. Theoretical studies by Hartnett and Eckert (ref. 17) and Cohen, Bromberg, and Lipkis (ref. 18) show enhanced convective heating caused by gas phase reactions between air and ablated vapors. Experimental results of Vojvodich and Pope (ref. 19) confirm that both heterogeneous and homogeneous combustion between air and charring ablators impose a heat load comparable to the net convective heating ($q_{co}\psi$) at low levels of shock-layer pressure ($10^{-3}$ to $10^{-2}$ atm) and driving enthalpies up to about 8000 Btu/$lb_m$. However, they show that the relative importance of combustion diminishes with increasing driving enthalpy and increasing pressure level. Very likely, the reason for diminished importance of surface reactions between air and ablation material is that higher injection rates prevent air from reaching the surface at the more extreme conditions. An analogous phenomenon was studied theoretically by Chung (ref. 20) in which he showed that heterogeneous recombination reactions are inhibited by air transpiration at a cold wall, preventing dissociated shock-layer air from reaching the surface. Further, the relative importance of energy release by gas phase reactions between air and injected species is diminished probably because of the increased energy release by recombination reactions of air components themselves at the more severe conditions.

Thus we assume that at the higher levels of shock-layer pressure ($10^{-1}$ to 10 atm) and higher enthalpies (20,000 to 50,000 Btu/$lb_m$) with which the present study is concerned, one need not sort out gas phase combustion reactions from other recombination reactions. So, we appropriate Lees argument mentioned previously and neglect the details of the combustion reactions but consider for practical purposes that their effects are included implicitly in $q_c$, the convective heating results.

At high flight speeds, radiative heating must be included with convective heating as causing ablation. The ablation rate for a given vaporizing material is related to the actual total heating flux, $q_T$, by

$$\sum (\rho_i \vec{V}_i)_w \left( \int_{T_m}^{T_w} c_{p_i} \, dT + h_{i_v} \right) = -q_T = -q_c - q_r \tag{5}$$

where the minus sign arises from the convention that positive flux is outward from the surface (that is, q means flux; it will be represented by a negative number if the wall is receiving heat), and the summation is over the ablation products appearing at the surface. The lower limit on the integral is $T_m$, the material temperature before heating began. Now we define the intrinsic heat of ablation as

$$h_a \equiv \frac{\sum \left( \rho_i \vec{V}_i \right)_w \left( \int_{T_m}^{T_w} c_{p_i} \, dT + h_{i_v} \right)}{\sum \left( \rho_i \vec{V}_i \right)_w} \tag{6}$$

The definition of the mass averaged velocity applied at the wall is

$$\rho_w v_w = \left( \rho_{air} \vec{V}_{air} \right)_w + \left( \sum \rho_i \vec{V}_i \right)_w \tag{7}$$

In order for air not to penetrate the surface, $\left( \rho_{air} \vec{V}_{air} \right)_w = 0$. Then combining equations (5), (6), (7), and (1) yields:

$$-q_T = \dot{m} h_a \tag{8}$$

In equation (5), $q_r$ is the net radiative heat flux accepted by the wall. It is a combination of the accepted incident radiative flux from the gas and the reradiated flux from the wall; thus

$$q_r = q_{r_g} + \epsilon_w \sigma T_w^4 \tag{9}$$

To express $q_T$ in a simple way, assume that (a) there is no coupling between radiative and convective heating rates (a very reasonable assumption for the application to moderate sized bodies made subsequently) and (b) $q_{r_g}$ is not a strong function of $-f_w$ or mass addition rate (which will be verified for conditions of special interest in the next section) and that (c)

$$q_{r_g} = -\alpha_w B R \tag{10}$$

where B is a constant for a given flight condition. Numerical solutions indicate that, for purposes of the estimates in this section, equation (10) is a good approximation even though the flow field is nonisoenergetic, as long as B is obtained from the nonisoenergetic solutions at a given flight

condition. Because no coupling is assumed (a) we can use the simple no blowing convective heating correlation (which, by the way, excludes external vorticity effects) of Hoshizaki (ref. 5) which can be put in the form

$$\frac{q_c}{\psi} = q_{c_o} = -4.03\times10^{-5}(2\epsilon)^{1/4}\bar{U}^{0.19}(j_s - j_w)\sqrt{\frac{p_s}{R}} \tag{11}$$

where the units on $4.03\times10^{-5}$ are $lb_f^{1/2}$ sec/$ft^{3/2}$ and the units on $q_{c_o}$ are $lb_f/ft^2$ sec. Combining equations (2), (5), (9), (10), and (11) leads to an expression for total heating rate

$$-q_T = \alpha_w BR - \epsilon_w T_w^4 + 4.03\times10^{-5}(2\epsilon)^{1/4}\bar{U}^{0.19}(j_s - j_w)\sqrt{\frac{p_s}{R}}\, e^{-b(-f_w)^n} \tag{12}$$

It is convenient to define

$$\left.\begin{aligned} A &\equiv \frac{\alpha_w B}{h_a\sqrt{\rho_s\mu_s U(k+1)}} \\ C &\equiv \frac{4.03\times10^{-5}(2\epsilon)^{1/4}\bar{U}^{0.19}(j_s - j_w)\sqrt{p_s}}{h_a\sqrt{\rho_s\mu_s U(k+1)}} \\ D &\equiv \frac{\sigma\epsilon_w}{h_a\sqrt{\rho_s\mu_s U(k+1)}} \end{aligned}\right\} \tag{13}$$

In terms of these quantities, equation (12) becomes

$$-q_T = h_a\sqrt{\rho_s\mu_s U(k+1)}\left[AR + \frac{C}{\sqrt{R}}\, e^{-b(-f_w)^n} - DT_w^4\right] \tag{14}$$

Now if equations (1), (5), (8), (9), (10), and (11) are combined, a transcendental expression is obtained for the natural blowing rate parameter $f_w$ in terms of R, the flight conditions, and material properties:

$$-f_w = AR^{3/2} + Ce^{-b(-f_w)^n} - DR^{1/2}T_w^4 \tag{15}$$

Another quantity of interest is the effective heat of ablation:

$$h_{eff} = \frac{-q_{T_o}}{\dot{m}} = -\frac{(q_{c_o} + q_{r_o})}{\dot{m}} \tag{16}$$

If we assume

$$q_{r_o} \approx q_r \tag{17}$$

which is approximately true for the moderate ablation rates which will concern us in this and the next section (and will be demonstrated at the end of the next section), it is simple to show that

$$\frac{q_T}{q_{T_o}} = 1 - \left[1 - e^{-b(-f_w)^n}\right] \frac{q_{c_o}}{q_{T_o}} \tag{18}$$

Combining equations (8), (13), (16), and (18) leads to

$$h_{eff} = h_a \left\{1 + \frac{C}{(-f_w)} \left[1 - e^{-b(-f_w)^n}\right]\right\} \tag{19}$$

where $-f_w$ is obtained from equation (15).

Now it is instructive to specialize some of these ablation relationships still further - to the case of convection only.

## Ablation Due to Convection Only

For flight speeds greater than satellite entry speed, both radiative and convective heating are important in determining ablation rates, even for small nose radii (which will be shown subsequently). However, if for the moment, convection is assumed to be the only heating mode, and both radiation and reradiation are excluded, we are led to some interesting comparisons. For these conditions, both equations (15) and (19) reduce to simpler forms, thus

$$-f_w e^{b(-f_w)^n} = C \tag{20}$$

and

$$\frac{h_{eff}}{h_a} = e^{b(-f_w)^n} = \frac{1}{\psi} \tag{21}$$

respectively. So we see that for the convective case, both the ablation rate in terms of $f_w$ (eq. (20)) and effective heat of ablation (eq. (21)) for a given material are independent of nose radius and ambient density (or pressure level), but depend only on flight speed (because $b$ is a function of $U$ alone (eq. (4)) and $C$ is essentially a function of $U$ because in equation (13)

$$(j_s - j_w)\sqrt{p_s/\rho_s\mu_s} \approx (U^3/2)\sqrt{\rho_\infty/\rho_s\mu_s}$$

and the last square root is a very weak function of ambient density). Lees (ref. 21) and Bethe and Adams (ref. 22) reached a similar conclusion for melting and glassy ablators at subsatellite speeds; that is, velocity is the important parameter.

It is interesting to compare this $f_w$ and $h_{eff}$ result obtained from $\psi$ that is exponential with respect to $(-f_w)^n$ (eq. (2)) with those obtained from $\psi$ that is linear with respect to $(-f_w)$ of reference 8. The $\psi$ of that paper written in terms of $f_w$ by use of equation (1) is

$$\psi = 1 - \beta \frac{(-f_w)(j_s - j_w)}{q_{c_o}} \sqrt{\frac{\rho_s \mu_s U(k+1)}{R}} \tag{22}$$

The corresponding $f_w$ for convection only (for that paper) obtained from equation (11):

$$-f_w = \frac{4.03\times10^{-5}(2\epsilon)^{1/4}\bar{U}^{0.19}(j_s - j_w)}{[h_a + \beta(j_s - j_w)]} \sqrt{\frac{p_s}{\rho_s \mu_s U(k+1)}} \tag{23}$$

or

$$-f_w = \frac{C}{1 + \frac{\beta}{h_a}(j_s - j_w)} \tag{24}$$

while $h_{eff}$ for the linear $\psi$ would be

$$\frac{h_{eff}}{h_a} = 1 + \frac{\beta}{h_a}(j_s - j_w) \tag{25}$$

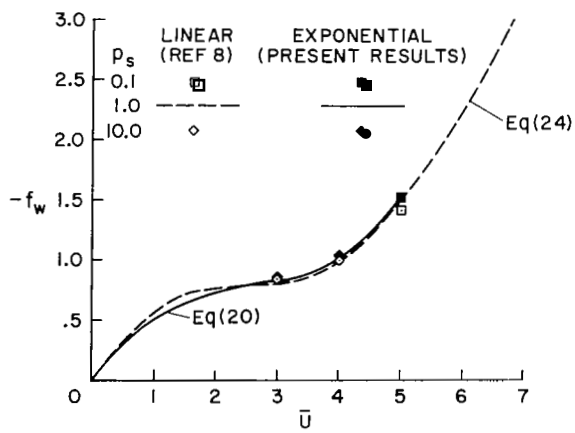


Figure 6.- Wall blowing parameter for natural ablation of Teflon at stagnation region - convection only.

The comparison of the natural $f_w$ for Teflon as predicted by the two results (eqs. (20) and (24)) is shown in figure 6[4] (using $\beta = 0.49$ and $h_a = 2.38\times10^7$ ft$^2$/sec$^2$ from ref. 8 for Teflon). It is seen that the two results are in close agreement and that both depend strongly on velocity, but not on pressure. Similarly, the results of $h_{eff}/h_a$ as a function of velocity are in close agreement for convection only (using eqs. (21) and (25)) as shown in figure 7.

The agreement between the two methods means that $e^{b(-f_w)^n}$ of equations (20) and (21) equals

[4]In this application and throughout the rest of the paper, the values of b and n for a given flight condition were obtained by passing equation (2) through results from the two flow-field solutions having the highest values of $-f_w$. Numerically, b and n are slightly different from expressions (3) and (4) for b and 3/2 for n obtained for the general correlation.

$1 + (\beta/h_a)(j_s - j_w)$. At first glance one might suspect that these natural blowing rates are small enough to be on the initial part of the $\psi$ curve where the exponential can be replaced by the first two terms of its series. It turns out that this is not the case as can be seen in figure 2. The solid curves and dashed lines correspond to the exponential and linear $\psi$ (to eqs. (2) and (22)), respectively, for the flight speeds shown. Although agreement between the solid curve and dashed line is better at the lower speeds, in neither case is the solid curve well represented by the dashed line except at the one point where they intersect. That intersection just happens to occur very near the natural value of $f_w$ in each case. Thus the apparent agreement in the results does not imply any general agreement in the function $\psi$ but, rather, is considered to be fortuitous.

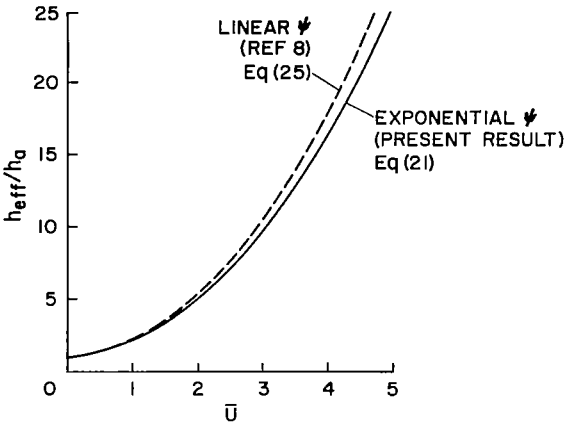


Figure 7.- Effective heat of ablation of Teflon (convection only).

Now we turn again to the case of ablation caused by both radiative and convective heating to examine some special conditions.

## Conditions at Minimum Heating Rate With Ablation

Because of the many combinations of variables, parameters, and phenomena associated with the ablation problem, it is convenient to seek an optimum condition, in terms of minimizing total heating rate or total mass loss rate of a given material at each flight condition, and then present some of the other quantities of interest correspondingly.

Nose radius and ablation rate for minimum heating rate.- Equation (14) shows that at a given flight condition, convective heating rate becomes large with small R whereas radiative heating rate becomes large at large R. Thus there is an intermediate value of R for which total heating rate is a minimum. This is illustrated graphically for one flight condition in figure 8. The family of solid light curves is calculated by use of equation (12) for specified values of $f_w$, and represents approximately the flow-field solution results. The family of dashed curves is calculated for Teflon by use of equations (8) and (1), also for specified values of $f_w$ (the physical properties used for Teflon and phenolic nylon are listed in table III). The intersection of a line of each family corresponding to one value of $f_w$ denotes a combination of $q_T$, R, and $f_w$ that satisfies

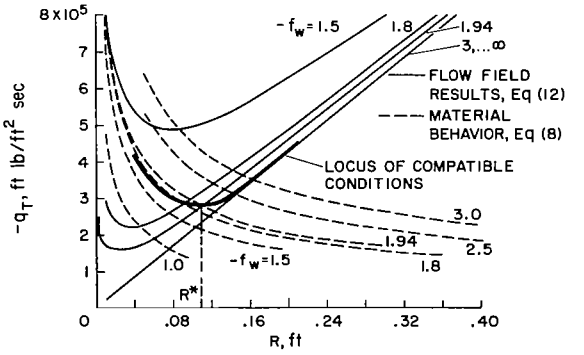


Figure 8.- Optimum nose radius for Teflon at U = 50,000 ft/sec, $p_s$ = 1 atm ($\alpha_w = \epsilon_w = 1$).

both the flow-field results and the material behavior. The heavy solid curve is the locus of such intersections. Its minimum gives the optimum nose radius $R^*$ which minimizes total heating rate (and total ablation rate) for Teflon for this flight condition. Thus $R^*$ is 0.109 foot and the ablation rate is given by $-f_w = 1.94$ in this example. The right branch of the heavy curve shows an interesting result. That is, for a nose radius half again as large as $R^*$, convective heating has been essentially eliminated by strong ablation, and thus $q_T$ increases linearly with $R$ and is independent of ablation rate ($-f_w = 3$ line coincides with $-f_w = \infty$), as it should be for radiative heating only, according to the approximation of equation (10). Correspondingly, ablation is caused by radiative heating alone and its rate must be increasing in proportion to $q_T$, and thus $R$, in accord with equation (8). This points out the potential importance of reflecting ablative surfaces for heat protection for radii greater than $R^*$.

Analytically, $R^*$ and $f_w$ for a specific material and flight condition are obtained as follows. The partial derivative of $q_T$ with respect to $R$ (obtained by differentiation of eq. (14) noting that $f_w$ is a function of $R$ by eq. (15)) is set to zero. After some algebra, the expression

$$f_w + \frac{Ce^{-b(-f_w)^n}}{2}\left[bn(-f_w)^n + 3\right] - DT_w^4 R^{1/2} = 0 \qquad (26)$$

is obtained. The simultaneous solution of equations (15) and (26) yields the optimum nose radius and natural ablation rate ($f_w$) for a given material and flight condition.

It can be noted that for no reradiation ($DT_w^4 R^{1/2}$ negligible), equation (26) is uncoupled from equation (15) and the former can be solved directly for $f_w$ after which the latter can be used to obtain the optimum $R$. Thus we obtain the result that $f_w$ is independent of the radiative properties of the gas expressed by $A$ in equation (13). Although $f_w$ depends only on the convective heating properties of the gas (expressed by $C$ in eq. (13) which appears in eq. (26)), it differs from the $f_w$ for convection only (eq. (20)) for the following reasons. If equation (15) is satisfied by $AR^{3/2} \neq 0$ by use of the $f_w$ obtained from equation (26), it cannot be satisfied for $AR^{3/2} = 0$ by the same $f_w$. Moreover, if radiation is zero, we cannot use equation (26) to calculate $f_w$ but must revert to equation (20).

For radiation different from zero but negligible reradiation, $h_{eff}$ is independent of the radiative flux because $f_w$ used in equation (19) is independent of radiative properties. The same is true for $\psi$ because of equation (2). On the other hand the optimum $R$ obtained from equation (15) depends on the radiative properties. Of course, $\dot{m}$ depends on the radiative properties because it depends on $R$ (eq. (1)), and the same is true for both $q_c$ (eq. (11)) and $q_r$ (eqs. (9) and (10)).

The optimum nose radius with convection, radiation, and reradiation obtained from equations (15) and (26) is shown as a function of flight speed

in figure 9 for Teflon and phenolic nylon. It can be seen that the optimum nose radius diminishes with increasing shock-layer pressure at a given flight speed. On the other hand, the optimum nose radius increases as flight speed is diminished, shock-layer pressure level being constant. These trends can be related to actual entry trajectories, by noting (ref. 1, fig. 1) that typical trajectories consist of essentially a path of increasing shock-layer pressure at constant velocity followed by a path of diminishing velocity at constant pressure. Now if the major heating occurs at constant velocity (the case of plunging probes), total heating rates could be minimized only by artificially tailoring the nose shape (for example, by pushing concentric rods of progressively smaller radii out the front of the vehicle in a programmed sequence - a refinement of a suggestion by H. J. Allen (ref. 23)). On the other hand, if the major heating occurs at constant shock-layer pressure (typical of g limited entry), the problem of minimizing total heating rates is simplified because R grows naturally in the direction of the growing optimum.

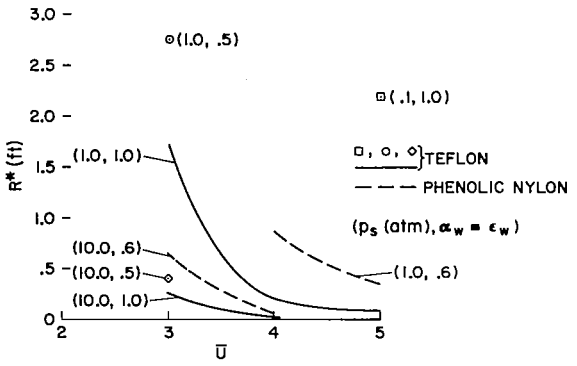


Figure 9.- Optimum nose radius for ablation.

The wall absorptivity, $\alpha_w$, is important to both charring and noncharring ablators because it influences the amount of radiant heat accepted from the gas cap and thus R*. In figure 9, if $\alpha_w$ is diminished by 50 percent for Teflon (noncharring), R* is increased by about 50 percent.

The wall emissivity is important to high-temperature charring ablators for which reradiation is an important heat rejection mechanism. For phenolic nylon, reradiation is partly responsible for a larger optimum nose radius than that of Teflon (for which reradiation is negligible because of its low vaporization temperature) - by about a factor of 3 in the speed range 40,000 - 50,000 ft/sec as can be seen in the figure. The phenolic nylon calculation for $p_s$ = 1 atm was not extended to lower speed because of the uncertain wall temperature; that is, the wall temperature becomes a function of the heating rate at less severe heating conditions.

The ablation rate, in terms of $f_w$, corresponding to optimum heating rate conditions is shown as a function of flight speed for various pressure levels and absorptivities for Teflon and phenolic nylon in figure 10. The heavy lines and symbols represent minimized total heating rate conditions, while the light

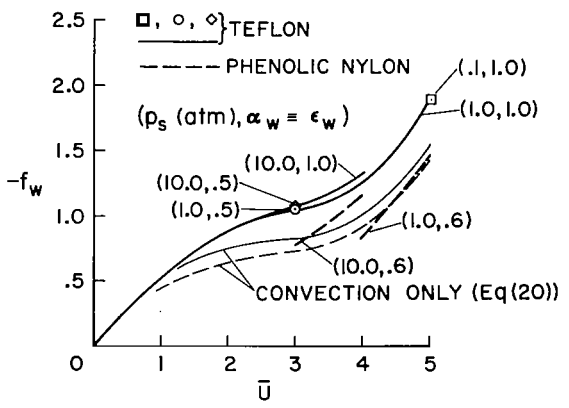


Figure 10.- Blasius wall blowing parameter corresponding to ablation with optimum nose radius.

lines represent the result for convection only (shown previously in fig. 6 for Teflon). It is important to point out that the difference between the total heating heavy lines and convective heating light lines does not represent the contribution of radiative heating. When minimum total heating rate is considered, there is a complete rearrangement of convective and radiative contributions. The result is that the radiative contribution is usually larger (sometimes much larger) than the convective contribution (which will be demonstrated subsequently in fig. 15). The result of the sum of the two readjusted heating components on $f_w$ is shown by the heavy lines in figure 10.

It is especially interesting to note that for Teflon, optimum $f_w$ is a very weak function of both absorptivity and pressure level. This will have consequences in figure 12 where it will be remarked upon.

The ratio of the surface mass flux to free-stream mass flux is related to $f_w$ by the Reynolds number. Thus

$$\frac{\dot{m}}{\rho_\infty U} = -f_w \sqrt{\frac{(k+1)}{\epsilon Re}} \tag{27}$$

It should be mentioned that $\epsilon^{1/2}$ is almost invariant with flight speed (between 30,000 and 50,000 ft/sec) at a given level of shock-layer pressure. It only varies at the worst from 0.233 to 0.278 as pressure level changes from 0.1 atm to 10.0 atm.

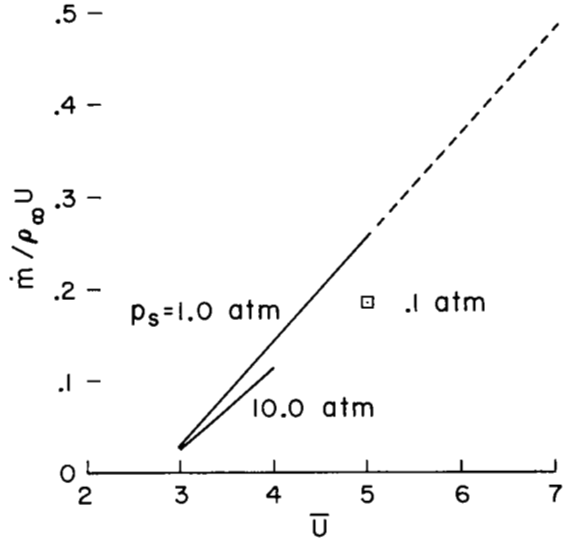


Figure 11.- Mass addition ratio for optimum conditions (Teflon, $\alpha_w = 1$).

The mass flux ratio of Teflon is presented in figure 11 for optimum conditions. The location of the point corresponding to 0.1 atm indicates that relationships at optimum conditions are not systematic in a simple way. The surface mass flux varies from 2-1/2 to 25 percent of the free-stream mass flux between 30,000 and 50,000 ft/sec. Some approximate calculations show that it is reasonable to extrapolate this result to 70,000 ft/sec. The result is that the mass flux ratio is still less than 0.5 for optimum conditions. This is in sharp contrast to the values in excess of unity for entry of some meteors for which the nose radius is very different from R* (Příbram meteor for example which likely has a radius of the order of a meter, ref. 24).

In fact, it is apparent from the present optimum results for U = 50,000 ft/sec and $p_s$ = 1 atm that if nose radius is increased from the optimum of 0.109 to only 0.5 foot, the mass loss ratio will exceed unity as a result of radiative heating alone.

Now that we have the nose radius which minimizes total heating rate, and the corresponding ablation rate, we can examine several other interesting quantities corresponding to these conditions.

Effective heat of ablation.- The ratio of the effective heat of ablation to the intrinsic heat of ablation is calculated by use of equation (19) and is presented in figure 12. The ratio depends strongly on velocity, but is relatively insensitive to pressure level (altitude) and, for the case of Teflon, surface absorptivity. The last is a consequence of the insensitivity of $f_w$ to $\alpha_w$ shown in figure 10, and the fact that $h_{eff}$ is very strongly dependent on $f_w$ in equation (19). The ratio $h_{eff}/h_a$ subject to combined radiative and convective heating is less than that obtained from convection alone, which can be seen by comparing figure 12 with figure 7.

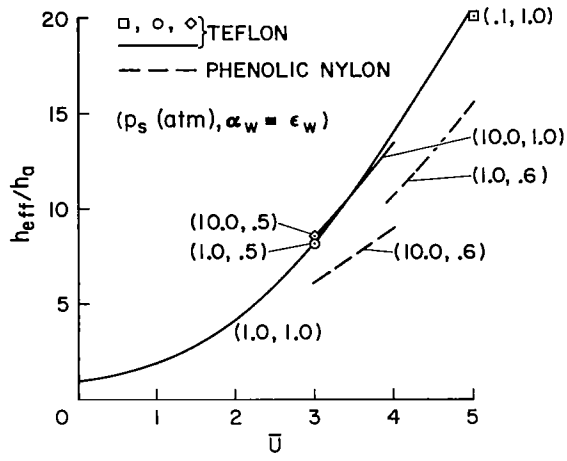


Figure 12.- Effective heat of ablation corresponding to natural ablation for optimum conditions.

In spite of the fact that $h_{eff}/h_a$ in figure 12 is smaller for phenolic nylon than for Teflon, the actual $h_{eff}$ for phenolic nylon is larger. At 50,000 ft/sec, the ratio of effective heat of ablation of phenolic nylon to that of Teflon is 1.13 which includes the reradiation effects. (It should also be remembered that the phenolic nylon is not ablating as rapidly as Teflon for these optimum conditions.)

Effect of mass addition on standoff distance.- The ratio of standoff distance with optimum mass addition (and nose radius) to that without mass addition was obtained by solving the flow-field equations using values of $R^*$ and $f_w$ obtained from figures 9 and 10. The result is shown in figure 13 for Teflon. For speeds below 30,000 ft/sec, where mass addition rates are low (3 percent of free-stream mass flux - fig. 11), the standoff distance with blowing is actually less than that without blowing (ratio is about 0.94). This interesting effect occurs at very low mass addition rates over a broad flight range and may be attributable to a cooling effect that increases the flow-field density (and diminishes standoff distance) more than enough to overcome the space required for the increase in mass flow in the flow field. At higher speeds, and thus higher ablation rates, the standoff

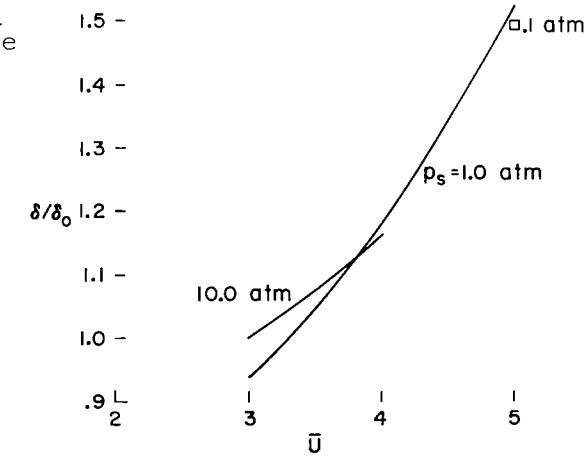


Figure 13.- Ratio of standoff distance with blowing to that without blowing for optimum conditions (Teflon, $\alpha_w$ = 1).

distance is enhanced by ablation. It is seen that for optimum conditions, the shock layer is thickened by about 50 percent at a speed of 50,000 ft/sec.

Effect of mass addition on radiative heating.- Mass addition can influence gaseous radiative heating flux in two ways; first, by altering the standoff distance and temperature distribution in the flow field (it should be mentioned that gaseous radiation reabsorption is negligible in the regime being considered), and, second, by adding chemical species to the flow field which radiate differently from air. To examine the first effect, due to alteration of flow-field structure, the foreign species was assumed to radiate like air. The resulting incident gaseous radiant flux at the wall as obtained from flow-field solutions corresponding to the optimum $R^*$ and $f_w$ of Teflon is compared with the no ablation value in figure 14. In the flight regime studied the maximum effect of the ablation on radiant flux is an increase of about 17 percent for these optimum conditions. This is in sharp contrast with the very large effects on convective heating presented earlier and supports the approximations of equations (10) and (17). For example, for flight condition in which radiative flux was changed 17 percent, ablation diminished the convective flux by two orders of magnitude (to 0.8 percent of its nonablation value).

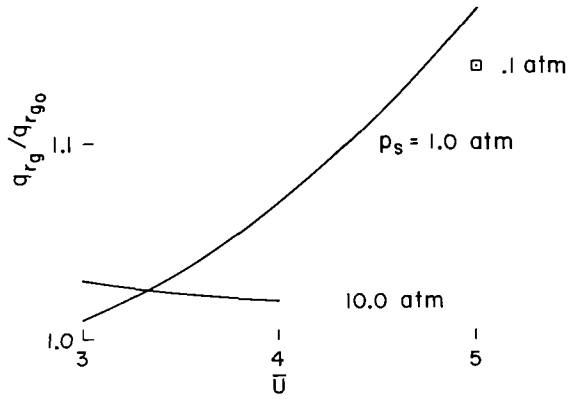


Figure 14.- Ratio of incident gaseous radiation flux with ablation to that without ablation at optimum conditions (Teflon, $\alpha_w = 1$).

To examine the second effect, that of introducing species which radiate differently from air, $\alpha$ in equation (A16) was specified to be different from unity. Briefly the result is that if a foreign gas that radiates twice as strongly as air ($\alpha = 2$) is introduced at the same rate, the radiative flux is enhanced at the most by only 5 percent over the air value. If the foreign gas radiates 10 times as strongly as air ($\alpha = 10$), the radiative flux is enhanced by about 50 percent over its airlike value at the most. Finally, the influence of these radiative properties that differ from those used in estimating optimum conditions on the optimum conditions themselves is as discussed previously. That is, to the extent that reradiation is negligible, there is no effect on $f_w$ and $h_{eff}$. However, the effect on $R^*$ is to reduce it by a factor of $1.5^{-2/3}$ (or 0.76) and the effect on $\dot{m}$ is to increase it by a factor of $1.5^{1/3}$ (or 1.14) at the worst by virtue of equations (15) and (1), respectively.

Comparison of radiative and convective heating.- The ratio of the radiative to convective heating rate was obtained from solutions of the flow-field equations in which $R^*$ and the $f_w$ corresponded to minimum heating conditions for Teflon. The result is that radiation exceeds convection by a factor

from 2 to 9 as shown in figure 15. The importance of convection increases as the level of shock-layer pressure is increased. For phenolic nylon, the results are almost the same without reradiation. That is $q_{r_g}/q_c$ is greater than unity. However, because of reradiation, the ratio $q_r/q_c$ is less than unity except at high pressures ($p_s$ = 10 atm). In any event, the gaseous radiant flux incident on the wall is considerably larger than the convective flux for either Teflon or phenolic nylon at optimum conditions.

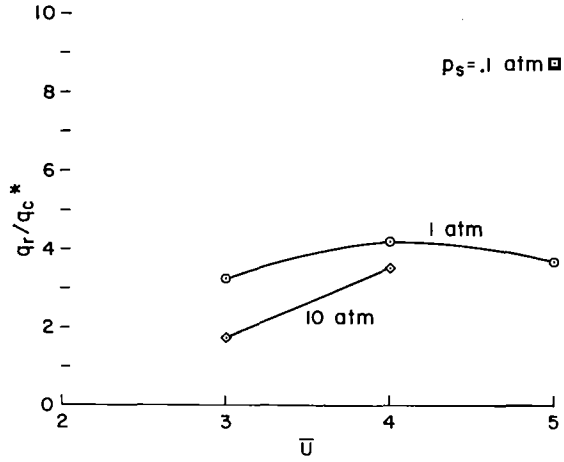


Figure 15.- Comparison of radiative and convective heating at optimum conditions (Teflon, $\alpha_w$ = 1).

Effect of mass addition on surface shear stress.- In figure 16, the surface shear stress divided by distance from the stagnation point is shown as a function of flight speed for various pressure levels for Teflon at optimum conditions. It was obtained from the flowfield solutions by use of the relationship

$$\frac{\tau_w}{x} = \varphi_w \left(\frac{U}{R}\right)^{3/2} \sqrt{(k+1)\rho_s \mu_s}\, f_w'' \qquad (28)$$

which can be derived by use of the transforms in appendix A. Generally, wall shear stress increases with velocity and shock-layer pressure level. For reasonable values of x, the shear stress is not excessive (even at $p_s$ = 10 atm, the surface shear stress per foot is of the order of standard atmospheric pressure per foot for optimum conditions, and the optimum size is considerably less than a foot). The shear stress for phenolic nylon would be slightly larger than that for Teflon because the mass addition rate for the former is lower at a given flight condition.

Of course, without mass addition, the shear stress would be considerably higher. The ratio of wall shear stress with mass addition to that without mass

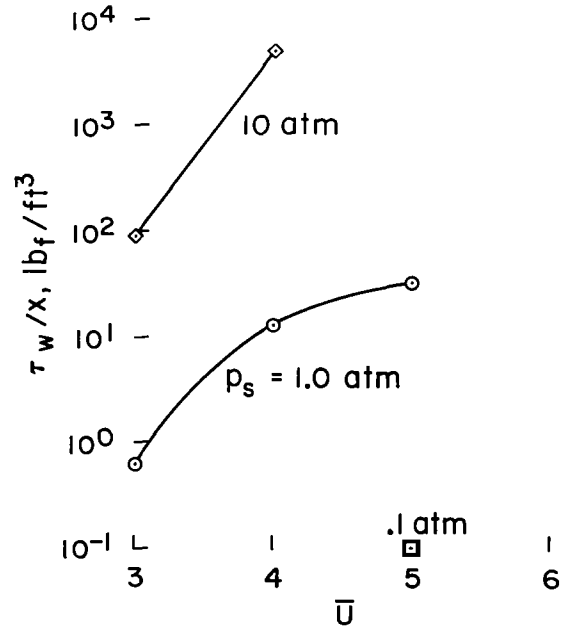


Figure 16.- Stagnation region shear stress at optimum conditions (Teflon, $\alpha_w$ = 1.0).

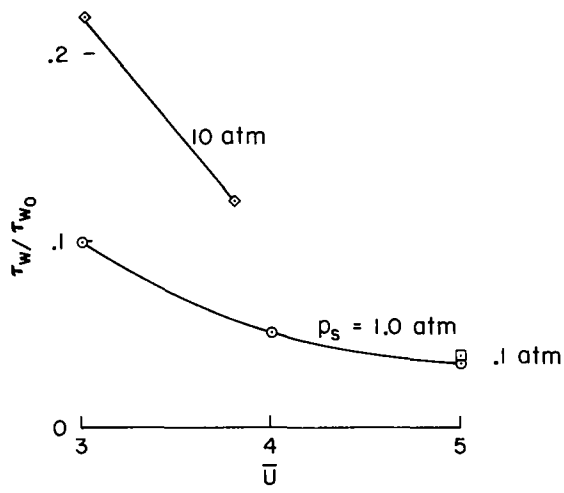


Figure 17.- Ratio of stagnation region shear stress with ablation to that without ablation at optimum conditions (Teflon, $\alpha_w = 1$).

addition is shown in figure 17 for Teflon under optimum conditions. It is noted that the ratio is only 0.035 at U = 50,000 ft/sec and $p_s$ = 1 atm.

Comments on validity.- Our optimum condition considerations have led to results of small nose radii for which the assumption of a flow field in chemical equilibrium may be doubtful. In spite of the fact that the chemistry and some of the thermodynamic and transport properties may be grossly in error for nonequilibrium flow fields, the basic structure of the flow field (velocity and enthalpy profiles) is not expected to be seriously in error. The reason is twofold: First, the analysis in the appendix of reference 25 shows that in the absence of transport phenomena, the enthalpy profile is almost unaffected by large departures from chemical equilibrium. Second, the velocity and enthalpy profile results of reference 26, which include both chemical nonequilibrium and transport phenomena, do not differ in a significant way from those of reference 1 or the present paper for chemical equilibrium (excluding low Reynolds number results).

Moreover, the convective heating is not likely to be very much in error because the wall is expected to be catalytic and thus nonequilibrium convective heating would be essentially the same as that for equilibrium since recombination would occur at or near the wall in either case.

We have noted that at the minimum heating condition, radiative heating dominates. Our radiative heating estimates could be in error for several reasons. Although the neglect of nonequilibrium radiation is a potential source of error for the small optimum nose radii, the present estimate is that it is not an important effect as gaged by the results of reference 27. We have already noted that there is some change in radiative heating caused by flow-field distortion and the presence of foreign species which radiate differently from air. Moreover, there is still considerable uncertainty in the radiative properties of air itself (the radiative properties of air given by ref. 28 may be high by a factor of 2 according to ref. 29) and in the absorptivities and emissivities of the surface material.

The effect of underestimating the radiative properties on optimum conditions has been noted in the section on effect of mass addition on radiative heating. Briefly, we now examine the effect of overestimating radiative properties by a factor of 2. As before, $f_w$, $h_{eff}$, and $\psi$ are unchanged (for a material which does not reradiate importantly). But $R^*$ is enhanced by about 60 percent, so $\dot{m}$ and $q_c$ are diminished by a factor $1.6^{-1/2}$ (or 0.79) by virtue of equations (1) and (11). So both $q_r$ and $q_c$ change, but in such

a way that $f_w$ is constant. The error in radiative properties by a factor of 2 has a large effect on $R^*$ (60 percent), only a 20-percent effect on $q_c$ and $\dot{m}$, and no effect on $f_w$, $h_{eff}$, and $\psi$.

Thus, in spite of the many uncertainties in the flow-field chemistry and in our knowledge of gas properties, the results of the minimized heating-rate study remain considerably meaningful.

## MASS ADDITION AND SCALING

To a large extent, experimental studies of high-speed planetary entry problems consists in exposing models to a simulated entry environment in a test facility, such as an arc-heated wind tunnel , a shock tube, or a ballistic range. Experimental results are then scaled to the actual flight conditions by one means or another.

Strictly speaking, we cannot expect to scale flow-field profiles at all because thermodynamic and transport properties used in the flow equations do not scale. However, in this portion of the paper, we will examine briefly how to scale dimensionless foreign species profiles approximately for forced mass addition (transpiration) and then specialize the result to natural mass addition (ablation).

### Scaling With Arbitrary Mass Addition

It is well known that in order to scale stagnation region flow fields in general, Reynolds number should be fixed. In order to scale foreign species concentration profiles, the mass addition rate must also be fixed. Or because of the Reynolds number factor in the expression relating $f_w$ and $\dot{m}/\rho_\infty U$ (and in view of the small variation in $\epsilon^{1/2}$ noted earlier), we may simply say that in order to scale mass addition effects, both $f_w$ and $\dot{m}/\rho_\infty U$ must be fixed. We will illustrate this by use of flow-field solutions.

The main points of the demonstration are briefly as follows. In figures 18 through 21, solutions corresponding to the conditions shown in table IV are presented in which either but not both $f_w$ or $\dot{m}/\rho_\infty U$ is the same between pairs of examples (assuming that these quantities can be varied at will). These results can be compared with those for which both $f_w$ and $\dot{m}/\rho_\infty U$ (or Re) are constant, shown in figures 22 through 25.

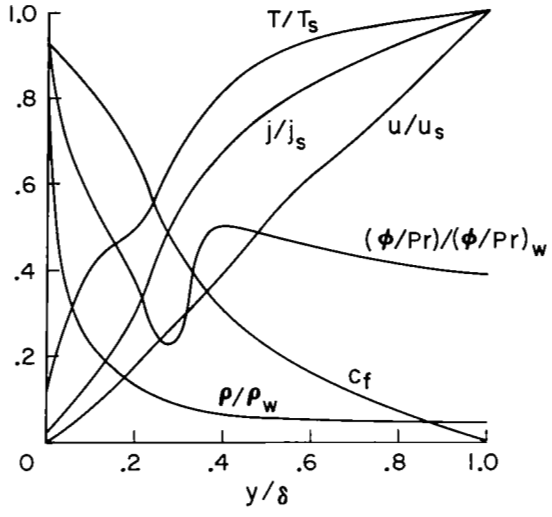


Figure 18.- Flow-field profiles;
U = 41,000 ft/sec, $p_s$ = 1 atm, R = 0.01 ft,
$f_w$ = -1.

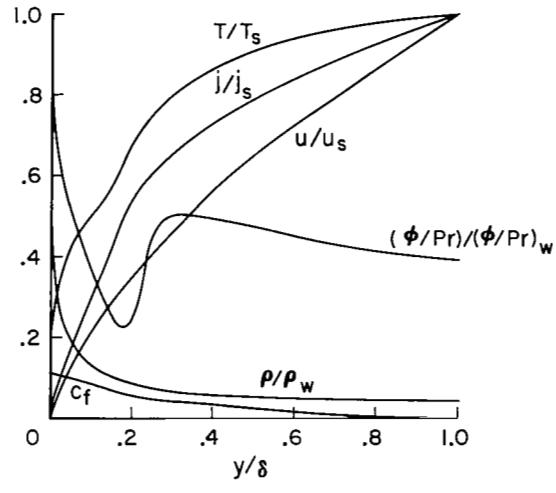


Figure 19.- Flow-field profiles;
U = 41,000 ft/sec, $p_s$ = 1 atm, R = 0.01 ft,
$f_w$ = -0.1.

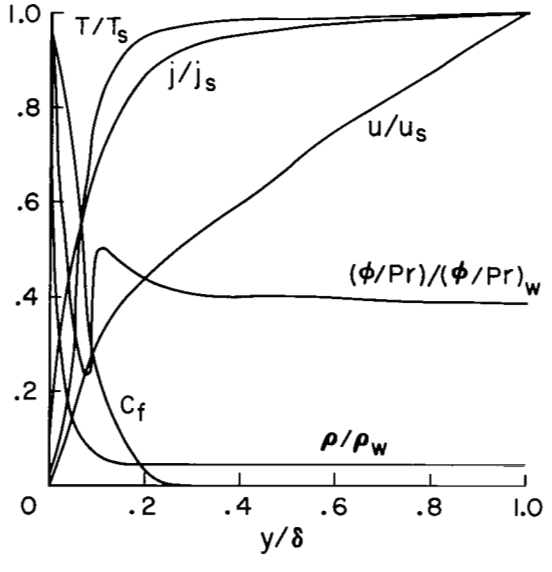


Figure 20.- Flow-field profiles;
U = 41,000 ft/sec, $p_s$ = 1 atm, R = 1 ft,
$f_w$ = -1.

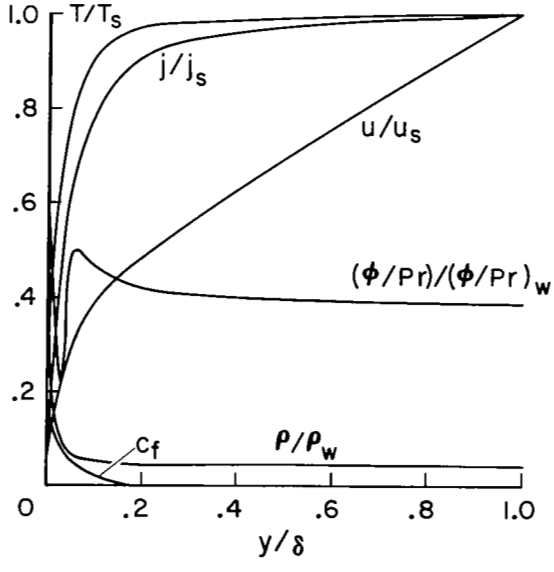


Figure 21.- Flow-field profiles;
U = 41,000 ft/sec, R = 1 ft, $p_s$ = 1 atm,
$f_w$ = -0.1.

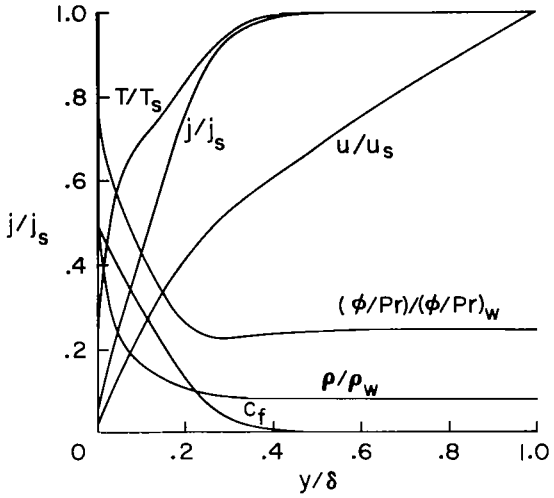


Figure 22.- Flow-field profiles;
U = 30,000 ft/sec, $p_s$ = 1 atm, R = 0.063 ft,
$f_w$ = -0.3.

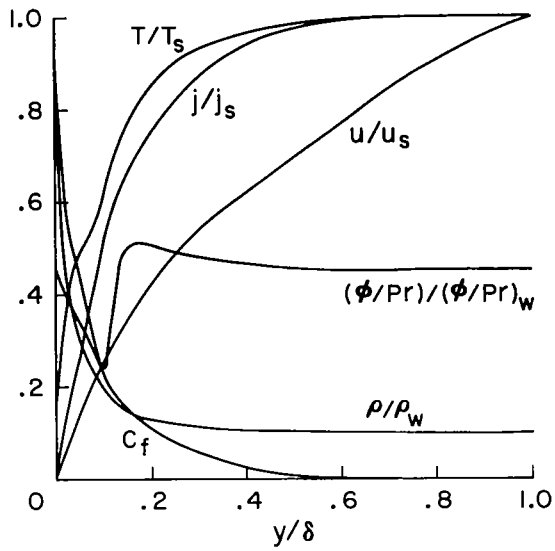


Figure 23.- Flow-field profiles;
U = 41,000 ft/sec, $p_s$ = 10 atm, R = 0.011 ft,
$f_w$ = -0.3.

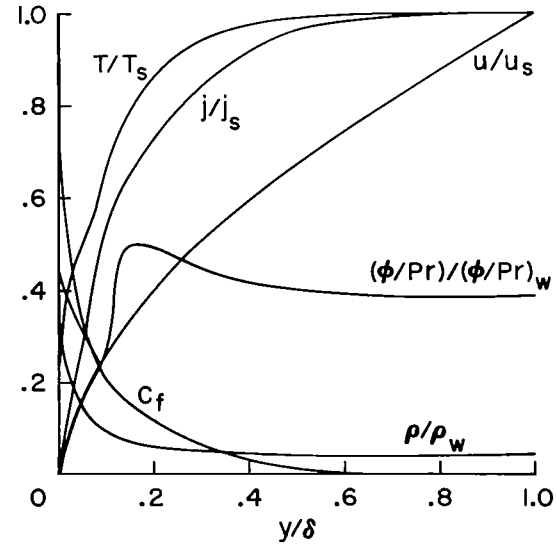


Figure 24.- Flow-field profiles;
U = 41,000 ft/sec, $p_s$ = 1 atm, R = 0.1 ft,
$f_w$ = -0.3.

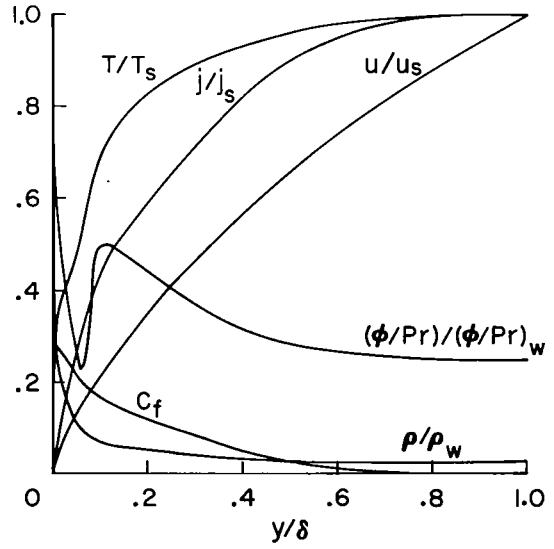


Figure 25.- Flow-field profiles;
U = 50,000 ft/sec, $p_s$ = 1 atm, R = 0.074 ft,
$f_w$ = -0.3.

The foreign species profiles corresponding to these two groups of figures are summarized in figure 26(a) and 26(b), respectively. Obviously the concentration profiles resulting from fixing only one of the parameters do not scale as can be seen in figure 26(a). The figure shows that $f_w$ essentially controls the foreign species concentration at the wall, while Reynolds number determines its penetration into the flow field. Thus, if both $f_w$ and Re (or $\dot{m}/\rho_\infty U$) are fixed, scaling should be much improved, as is evidenced by the $c_f$ profiles summarized in figure 26(b). Moreover, since fixing $f_w$ and $\dot{m}/\rho_\infty U$ essentially preserves Reynolds number (the slight variations in Re in table IV are caused by variations in $\epsilon^{1/2}$ in eq. (27)), the velocity profiles of the second set (figs. 22 - 25) are scaled; where in the first set (figs. 18 - 21) they are not. Finally, the enthalpy profiles of the first set exhibit less similarity than those of the second set. The latter are summarized in figure 27.

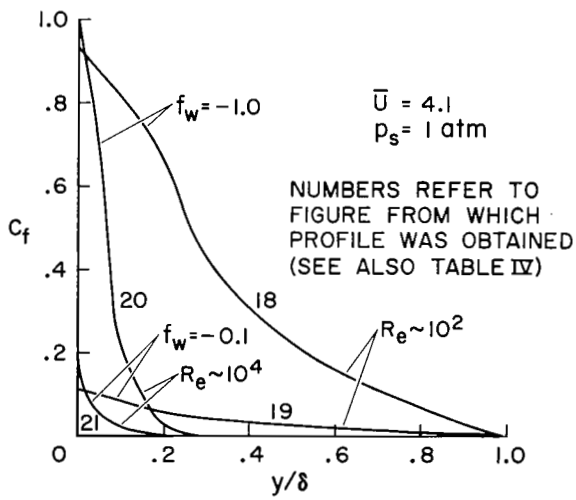


(a) Either $f_w$ or $\dot{m}/\rho_\infty U$ fixed.

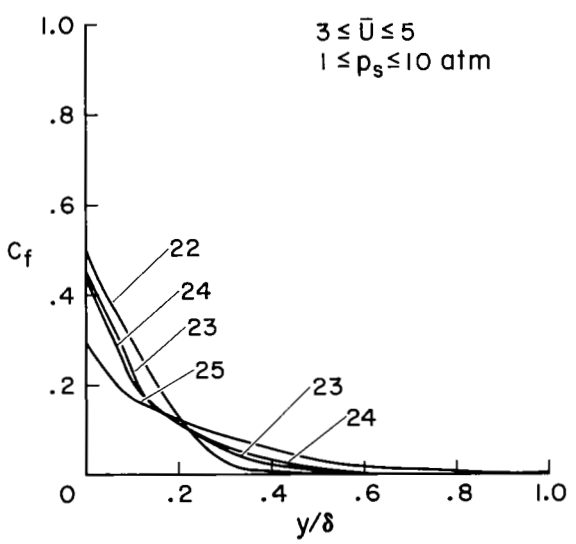


(b) Both $f_w$ (= -0.3) and $\dot{m}/\rho_\infty U$ (= 0.05) fixed.

Figure 26.- Foreign species concentration profiles.

There are additional features of some of the solutions mentioned above which, although secondary to the argument, are worth comment. In figure 18, for a flight condition of U = 41,000 ft/sec and $p_s$ = 1 atm, a nose radius of 0.01 ft., and a blowing rate $f_w$ = -1.0, both momentum (associated with $u/u_s$ profile) and thermal (associated with $j/j_s$ profile) boundary layers are conspicuously absent. Indeed, the vorticity (slope of $u/u_s$ curve) is approximately constant throughout the flow field. Interestingly, the flow field is far from isoenergetic everywhere; not because of enthalpy

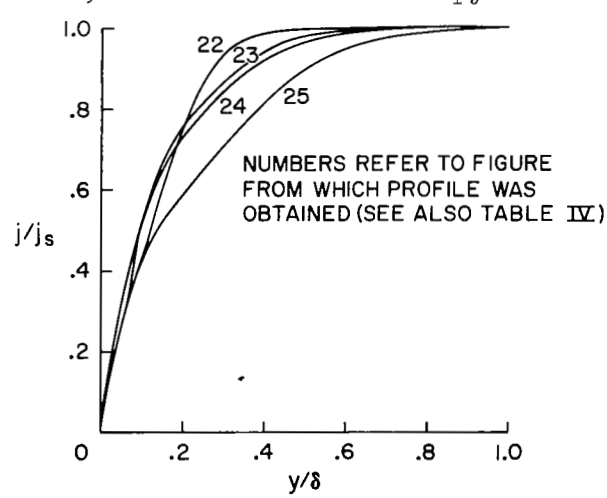


Figure 27.- Comparison of enthalpy profiles for both $f_w$ ( = -0.3) and $\dot{m}/\rho_\infty U$ ( = 0.05) fixed.

depletion by radiation but, rather, by convection. The mass addition rate at the surface is half the free-stream mass flux (table IV), and standoff distance is 90 percent higher than the no-blowing value (this is the most extreme result that we have in both regards). The foreign species completely permeates the flow field, which is important from the point of view of the relative importance of air and ablation species radiation. In this regard, results show that the incident gaseous radiant heating flux at the wall is enhanced by 49 percent over the no-blowing value if air is the injected gas (because of the thickened shock layer), but is enhanced by 93 percent over the no-blowing value if a species that is three times as strong an absorber and emitter as air ($\alpha = 3$ in eq. (A16)) is injected at the same rate. If the mass addition rate is diminished by a factor 1/10, the principal effect is to greatly diminish the foreign species concentration (fig. 19). However, the foreign species still permeates the entire flow field because Re is moderately low ($\sim 10^2$).

Now if we increase body size (going from figs. 19 to 20), the result is that we regain the structure of both a momentum and thermal boundary layer (i.e., there are large changes in $u/u_s$ and $j/j_s$ near the wall). The foreign species vanishes at only a third of the distance from the wall to the shock in spite of the fact that its concentration at the wall is an order of magnitude larger than that of figure 19 and the mass addition rate is the same. These are all the effects of going to a larger Reynolds number ($\sim 10^4$ in table IV), and they underscore the importance of preserving (at least approximately) the Reynolds number in scaling mass addition effects.

Now we specialize the scaling discussion to the ablation case.

## Scaling With Ablation

Although it is generally not possible (and sometimes not desirable) to simulate or scale all of the pertinent parameters in the laboratory, it is nevertheless worth examining the extent to which mass addition can be scaled in the presence of conduction, gas and surface radiation, and ablation.

Conduction, radiation, and reradiation.- The expression for the material $f_w$ as obtained from equations (15) and (13) can be written

$$-f_w = \frac{1}{h_a}\sqrt{\frac{Re}{\epsilon(k+1)}}\left[\alpha_w B(U,\rho_s)\frac{R}{\rho_s U} + 2.015\times10^{-5}(2\epsilon)^{1/4}\bar{U}^{0.19}U^2\sqrt{\frac{\epsilon}{\rho_s R}}\,e^{-b(-f_w)^n} - \frac{\sigma\epsilon_w T_w^4}{\rho_s U}\right] \tag{29}$$

We confine our attention to one material and assume that $h_a$, $\alpha_w$, $\epsilon_w$, and $T_w$ are constant and, moreover, that $\epsilon$ and $\bar{U}^{0.19}$ are almost constant. Then, in order to scale the flow-field concentration, we require (from the preceding section), that both $f_w$ and $\dot{m}/\rho_\infty U$ be fixed; or, alternatively, we require both $f_w$ and Re be fixed. From equation (29) these can be fixed if the

brackets in equation (29) are fixed. Conceivably, one could find a range of flight conditions and nose radii for which the bracket and $f_w$ within the bracket are fixed. The constancy of the bracket would then constitute a somewhat unappealing scaling law. It could be specialized to a set of simple laws, namely that

$$\frac{RB(U,\rho_s)}{\rho_s U}, \qquad \frac{U^2}{\sqrt{\rho_s R}}\, e^{-b(-f_w)^n}, \qquad \text{and} \qquad \frac{1}{\rho_s U}$$

are individually constant, where these pertain to radiative, convective, and surface reradiative transport, respectively. If convective heating is negligible, we can scale by keeping $\rho_s U$ and RB fixed between model and prototype.

Note that, in general, we cannot have constant velocity scaling with this set of simple laws; that is, $\rho_s$ and (because $b = b(U)$) R must be individually constant so that there is no hope of scaling either flow field or model to achieve foreign species scaling. Even if we neglect either radiative or convective heating we cannot have constant velocity scaling because of the surface reradiative term.

Radiation only.- If this is the only energy transfer mode, scaling can be accomplished if $f_w$ and Re are constant which requires that $BR/\rho_s U$ be constant. Or the last can be replaced by constant $BR^2/\mu_s$ because Reynolds number is fixed. For scaling at constant velocity, $BR/\rho_s$ must be constant.

Convection only.- This situation is especially applicable to ground-based tests with noncharring ablation models in arc-heated wind tunnels and ballistic ranges. If this heating mode is assumed to prevail also for the prototype at actual flight conditions (as was the case for the mass addition calculation of ref. 30), the scaling law requires that either $(U^2/\sqrt{\rho_s R})e^{-b(-f_w)^n}$ or $(U^{5/2}/\sqrt{\mu_s})e^{-b(-f_w)^n}$ be constant (as well as constant Re and thus constant $f_w$). For constant velocity scaling, the requirement is simply that $\sqrt{\mu_s}$ be constant (along with Re). Since $\sqrt{\mu_s}$ is a weak function of altitude for constant velocity, the conclusion is that $\dot{m}/\rho_\infty U$ is constant and the foreign species profiles are scaled simply if Re is preserved. T. N. Canning and G. Chapman of Ames Research Center have advanced the former conclusion ($\dot{m}/\rho_\infty U$ constant for constant Re) based on phenomenological arguments under the same constraints (simulated shape, Reynolds number, velocity, and noncharring material (no reradiation)), and for convection only.

In short, then, ablation scaling (by simple rules) in terms of ratio of mass flux at the wall to that in the free-stream and foreign species concentration profile can best be achieved for very special heating conditions. Constant velocity scaling cannot be achieved for materials which reradiate importantly.

## Low Reynolds Number Effects Without Mass Addition

It is common to study mass addition effects on convective heat transfer by use of the effective heat of ablation and a heating rate corresponding to no mass addition. For large Reynolds number (no shock-layer vorticity) and high speeds (up to 50,000 ft/sec), the convective heating rate without mass addition is quite well known both by experiment (refs. 31, 32, 5, 33, and 34) and theory (refs. 5, 35, 1, and 36). Moreover, a number of investigators have studied the regime of Mach numbers up to 8, where Reynolds numbers are low enough that shock-layer vorticity affects the convective heating rate for no mass addition (refs. 37-43). Van Dyke (refs. 44 and 45) has studied the vorticity effect up to infinite Mach number without real gas effects. Hoshizaki (ref. 46) has examined the vorticity effect for the incompressible shock layer. Our intent is to examine briefly the external vorticity (or low Reynolds number) effect on wall shear stress and convective heat transfer at high speed using real gas properties.[5]

Surface shear stress.- The present flow-field analysis is a single layer analysis in which the equations are solved from the body to the shock. A very simple comparison of the single layer result with the no vorticity two layer (boundary layer plus inviscid shock layer) result for surface shear stress can be made as follows.

The single layer shear stress has been expressed by equation (28). It is simple to show for the two layer no vorticity analysis for a cold wall (ref. 1, for example) that

$$\left(\frac{\tau_w}{x}\right)_{\text{no vort}} = \left(\frac{U}{R}\right)^{3/2} \frac{(2\epsilon)^{3/4}\sqrt{\rho_w\mu_w(k+1)}\,F_w''}{2\sqrt{2}} \tag{30}$$

where $F_w''$ is the value at the wall corresponding to the solution of the Blasius equation for no mass addition, and is given by reference 47. The ratio of $\tau_w/\tau_{w\,\text{no vort}}$ obtained by combining equations (28) and (30) is

$$\frac{\tau_w}{(\tau_w)_{\text{no vort}}} = \frac{2\sqrt{2}\,(\varphi_w)^{1/2}}{(2\epsilon)^{3/4}}\frac{f_w''}{F_w''} \tag{31}$$

---

[5]Because of a conflict which arises in the outer boundary conditions for very small Reynolds numbers, the results of this section and those of figures 18 and 19 are considered to be first approximations. The conflict is discussed and evaluated in an approximate way in appendix B.

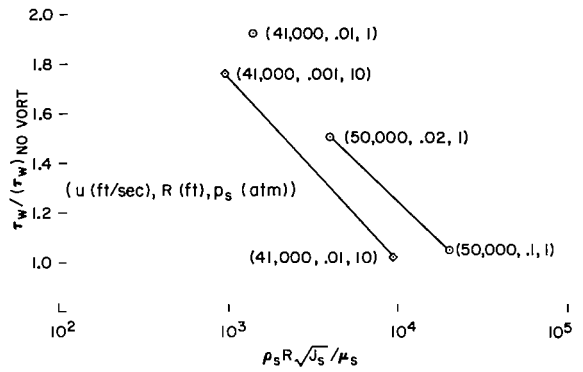


Figure 28.- Effect of Reynolds number on surface shear stress with no mass addition.

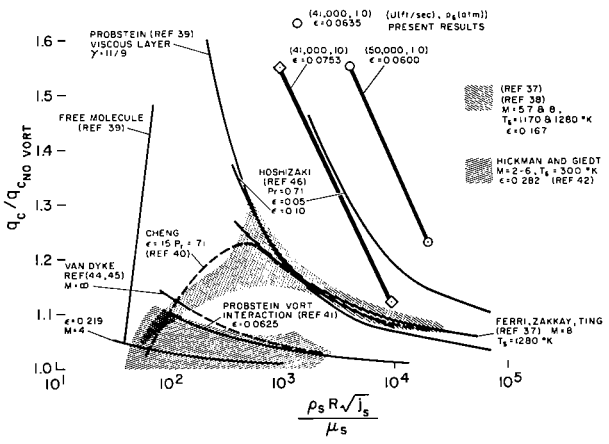


Figure 29.- Effect of Reynolds number on convective heat transfer with no mass addition.

The result is shown in figure 28 in which the ratio is plotted as a function of Reynolds number of the form used by reference 38. As would be expected, shear stress increases over its no vorticity value as Reynolds number decreases. At a given Reynolds number, the effect is enhanced by increasing speed and decreasing pressure.

Convective heat-transfer rate.- The convective heat-transfer results for the same examples are shown in figure 29. For present purposes, $q_{c_{no\ vort}}$ was obtained by use of equation (11) which is the result of Hoshizaki (ref. 5). It can be noted that the convective heating result parallels the shear stress result as would be expected.

The theoretical and experimental results of others (as obtained from refs. 38, 43, and 46) are shown for comparison. In each separate study the ratio of convective heating with vorticity to that without is enhanced by increase in speed or Mach number (M) or (for the case of ref. 46) $\epsilon$ at a given Reynolds number. Among the various studies, the ratio does not always increase with Mach number and there is some disagreement as to the reason (discussed in refs. 37, 43, and 45). The present results lie considerably higher than those of references 38, 40, 42, 44, and 45 as would be expected because of our comparatively high speed (or Mach number) and/or low $\epsilon$.

Our results are close to the viscous layer results of Probstein (ref. 39) and Hoshizaki (ref. 46). The results of these three studies are all derived from flow field analyses which employed the Navier Stokes equations from the body to the shock wave. Both Probstein and Hoshizaki assumed constant density and Prandtl number. Our results lie above theirs for a given Reynolds number and $\epsilon$ possibly because of our variable Prandtl number corresponding to higher speeds for which ionization occurs, and possibly because of compressibility effects near the cold wall. The slopes of our lines are alike and are much like those of Hoshizaki at lower Reynolds numbers. The vorticity results show that convective heating may be as much as 60 percent higher than the no vorticity value and that the ratio of the two is enhanced by increased U or diminished $p_s$ (or $\epsilon$) at constant Reynolds number.

The ratio of convective heat-transfer rate to total free-stream energy flux for these same examples is shown as a function of Reynolds number in figure 30. The results of references 37 and 38 at Mach numbers 5.7 and 8 are also shown. In each case the slanted line corresponds to the no vorticity result. At a given Reynolds number, $C_H$ without vorticity increases with in increasing speed. The symbols represent the present result and are attached to the appropriate no vorticity line by a vertical line. Conservation of energy requires $C_H$ be not more than unity. Thus $C_H$ of unity represents the flow energy limit. For the examples represented by the symbols, the convective heating was less than half the flow energy limit at the most.

Finally, flow-field solutions for some of the nonablating small body points of figures 28, 29, and 30 are shown in figures 31, 32, and 33. The

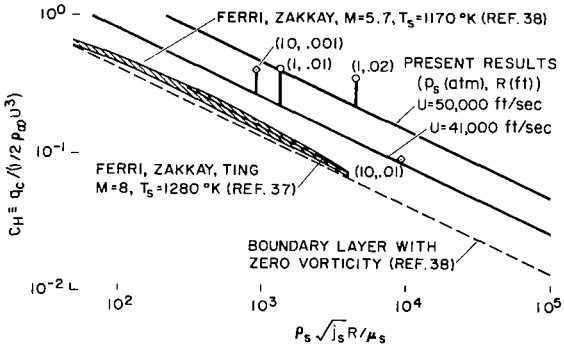


Figure 30.- Effect of Reynolds number on heat-transfer coefficient for no mass addition.

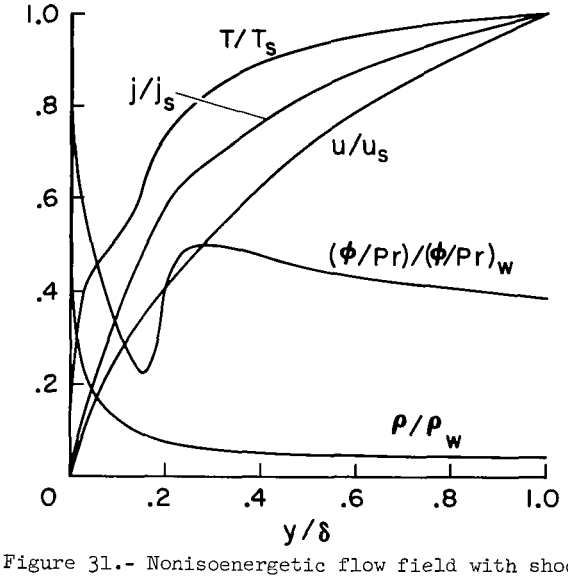


Figure 31.- Nonisoenergetic flow field with shock layer vorticity for no mass addition (U = 41,000 ft/sec, $p_s$ = 1 atm, R = 0.0104 ft).

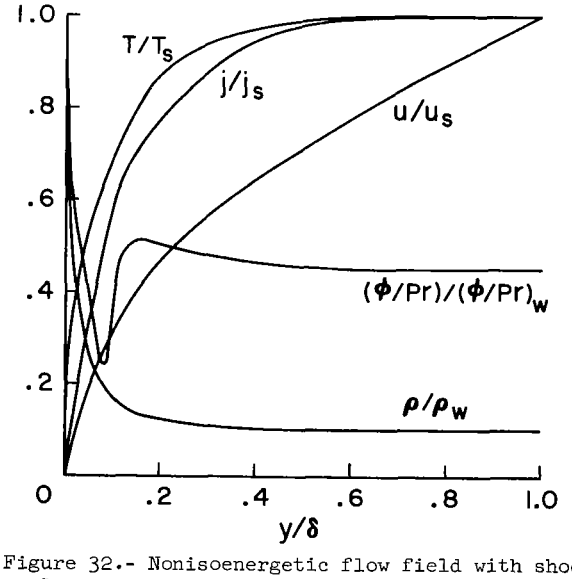


Figure 32.- Nonisoenergetic flow field with shock layer vorticity for no mass addition (U = 41,000 ft/sec, $p_s$ = 10 atm, R = 0.01 ft).

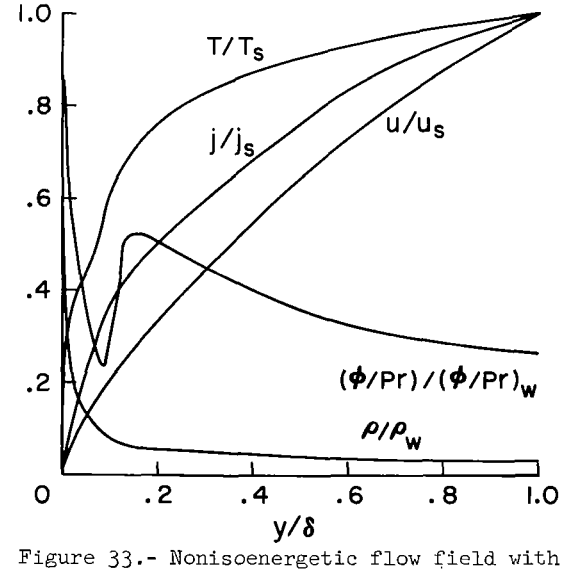


Figure 33.- Nonisoenergetic flow field with shock layer vorticity for no mass addition (U = 50,000 ft/sec, $p_s$ = 1 atm, R = 0.02 ft).

trend toward increased vorticity near the wall relative to that near the shock, and toward a more nearly isoenergetic flow field behind the shock for higher pressure can be seen from comparison of figures 31 and 32.

## CONCLUDING REMARKS

The flow equations in the stagnation region of the shock layer of blunt bodies (including mass, momentum, and energy transport phenomena) have been solved for numerous examples at flight speeds up to 50,000 ft/sec in air. The thermodynamic and transport properties of dissociating ionizing air were used in the analysis.

Many results with mass addition (by transpiration or ablation) were obtained. It was shown that convective heating was more strongly affected by mass addition than was radiative heating for mass addition rates up to half the free-stream mass flux (excluding effects of radiation from ablation products). Convective heating results were correlated by a simple relation which shows that mass addition diminishes convective heating exponentially, where the argument of the exponential is a simple function of flight speed and Blasius type wall stream function to the 3/2 power, $(-f_w)^{3/2}$. Results with mass addition for body nose radii between 0.01 and 5.0 feet, flight speeds from 30,000 and 50,000 ft/sec, wall temperatures from $1500^{\circ}$ to $3000^{\circ}$ K, shock-layer pressure levels from 0.1 to 10.0 atmospheres, and surface mass addition rates up to half the free-stream mass flux were correlated by the simple expression.

Previous correlation formulas obtained from subsatellite speed results do not correlate the present higher speed convective heating results corresponding to high mass addition rates.

The results with mass addition were used to study ablation at hypervelocity for which convection, gaseous radiation, and surface reradiation were taken into account. At specified flight conditions (ranging in speed between 30,000 and 50,000 ft/sec and between 0.1 and 10.0 atm shock-layer pressure level) for a given ablator, the nose radius which minimizes total heating rate was determined. For this "optimum" nose radius, the following results were obtained.

1. The ablation rate in terms of the stream function at the wall depends only on the convective heating properties of the gas and is independent of the gaseous radiation properties if reradiation from the surface itself is negligible.

2. The ablation rate in terms of mass flux at the surface is not more than one fourth the free-stream mass flux for the flight regime cited above and is not more than half the free-stream mass flux at a speed of 70,000 ft/sec.

3. The influence of mass addition on standoff distance is moderate, the distance being enhanced by not more than 50 percent over its no-ablation value.

4. The gaseous radiation flux incident on the surface is larger than the conduction flux by a factor of 2 to 9.

5. If the ablated vapors radiate like air, mass addition enhances the incident radiant flux at the surface by less than 20 percent over the no-ablation value.

6. If the ablated vapors radiate 10 times as strongly as air, mass addition enhances the incident radiant flux at the surface by less than 50 percent over the airlike value.

7. The surface viscous shear stress is low; generally not more than 5 percent of the surface pressure.

In order to scale mass addition effects in terms of dimensionless concentration profiles of the foreign species, it is necessary to match both Reynolds number and either the stream function at the wall or the ratio of the mass flux at the wall to that of the free stream.

Ablation rate and foreign species concentration profiles can be scaled conveniently for very special heating conditions only. Constant velocity scaling cannot be achieved for materials which reradiate importantly.

Finally, at low Reynolds numbers, the shock-layer vorticity enhances both shear stress and convective heating over the no-vorticity values, the effect being greater at higher speed and lower pressure.

Ames Research Center
National Aeronautics and Space Administration
Moffett Field, Calif., May 18, 1964

## APPENDIX A

## FLOW-FIELD THEORY

The formulation of the flow-field analysis is the same as that described in reference 1. We consider the stagnation region flow field as a whole without subdividing it into a viscous nonadiabatic boundary layer and an inviscid adiabatic shock layer. The analysis includes the effects of viscosity, heat conduction, diffusion, emission and absorption of radiation, and takes into account that the gas is both dissociated and ionized. The principal assumption is that the gas is in chemical equilibrium.

### DIFFERENTIAL EQUATIONS

The coordinate system for the analysis is shown in sketch (a). In the stagnation region,

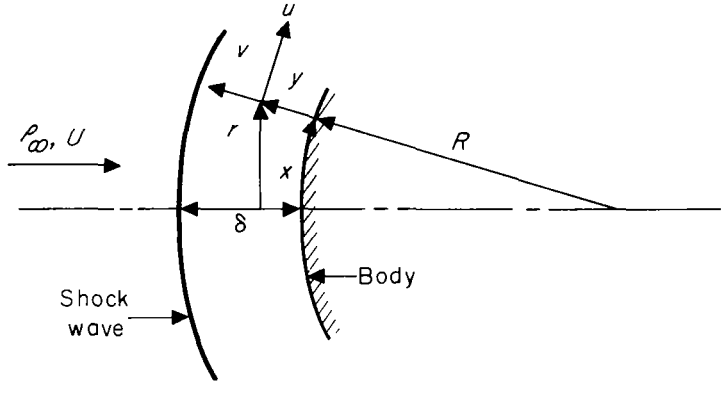


Sketch (a)

$$r(x,y) = Hx \tag{A1}$$

where

$$H = 1 + (y/R) \tag{A2}$$

The equations of mass conservation, momentum, energy, and diffusion are

$$\frac{\partial}{\partial x}(\rho u r^k) + \frac{\partial}{\partial y}(H\rho v r^k) = 0 \tag{A3}$$

$$\rho u \frac{\partial u}{\partial x} + H\rho v \frac{\partial u}{\partial y} = - \frac{\partial p}{\partial x} + H \frac{\partial}{\partial y}\left(\mu \frac{\partial u}{\partial y}\right) \tag{A4}$$

$$\rho u \frac{\partial v}{\partial x} + H\rho v \frac{\partial v}{\partial y} - \frac{\rho u^2}{R} = -H \frac{\partial p}{\partial y} \tag{A5a}$$

$$\rho u \frac{\partial j}{\partial x} + H\rho v \frac{\partial j}{\partial y} = H \frac{\partial}{\partial y}\left(\frac{\mu}{Pr} \frac{\partial h}{\partial y}\right)$$

$$+ H\rho K \left[ \int_o^{t_s} 2\sigma T^4(t) E_1(|t - \tau|)dt - 4\sigma T^4 + 2\sigma T_w{}^4 E_2(\tau)\right] \tag{A6}$$

and

$$\rho u \frac{\partial c_f}{dx} + H\rho v \frac{\partial c_f}{\partial y} = H \frac{\partial}{\partial y}\left(\rho D_f \frac{\partial c_f}{\partial y}\right) \tag{A7}$$

A detailed discussion of these equations appears in reference 1. In it, arguments were advanced to justify replacing equation (A5a) by

$$\frac{\partial p}{\partial y} = 0 \tag{A5b}$$

However, for the case of mass addition at high rates, this replacement must be examined more closely. If we confine attention to the stagnation region, where $x \approx \delta$ and for order of magnitude estimates say $u \sim Ux/R$, $\rho \sim \epsilon^{-1}\rho_\infty$, $p \sim \rho_\infty U^2$, $\partial v/\partial x \sim \epsilon Ux/R^2$, and $x/R$ is of the order of $\epsilon$, the terms in equation (A5a) are of the size

$$\epsilon^3 + \epsilon \frac{R}{U}\left(\frac{\rho_v}{\rho_\infty U} \frac{\partial v}{\partial y}\right) - \epsilon^2 = - \frac{\Delta p}{p}$$

respectively, where $\Delta p$ is the change in pressure across the shock layer in the $y$ direction. Now if $\rho_v/\rho_\infty U$ is of the order unity and $\partial v/\partial y \sim \epsilon U/\delta$, the result is that $\Delta p/p$ is of the order $\epsilon$. Thus it is reasonable to replace equation (A5a) with equation (A5b) for mass addition rates not in excess of $\rho_w v_w = \rho_\infty U$ because (1) the pressure level across the shock layer changes only of the order $\epsilon$ and (2) only the pressure level and not its gradient normal to the wall is needed in the rest of the analysis. The advantage of being able to use equation (A5b) rather than (A5a) is enormous. Because of it, the effects of conduction and diffusion have been combined by use of an equivalent total thermal conductivity (refs. 48 and 49) which is contained in the Prandtl number.

On the other hand, if $\rho_w v_w \gg \rho_\infty U$ (which is the case considered in ref. 50), the y momentum equation (A5a) must be retained and the energy equation (A6) cannot be written as it stands.

Finally, the radiation term in brackets in equations (A6) corresponds to the assumptions of a grey gas,[1] black surface, and plane parallel shock layer.

The following definitions are needed:

$$j = h + \frac{u^2 + v^2}{2} \tag{A8}$$

$$h = \sum c_i h_i \tag{A9}$$

$$h_i(T) = \int_o^T c_{p_i}\, dT + h_i^o \tag{A10}$$

$$\tau = \int_o^y \rho K\, dy \tag{A11}$$

$$E_n(\delta) = \int_1^\infty \frac{e^{-\delta\omega}}{\omega^n}\, d\omega \tag{A12}$$

$$\epsilon = \rho_\infty / \rho_s \tag{A13}$$

Boundary conditions for equations (A3) to (A7) are

---

[1]For the examples considered in the present paper, reabsorption of gaseous radiation for the grey case is of secondary importance. For this "transparent" condition, it can be shown that the use of the grey gas approximation with the Planck mean mass absorption coefficient leads to the correct total gaseous radiation flux. Moreover, the local energy depletion in the flow field by gaseous radiation (and coupling between radiative and convective heat transfer) are also given correctly under these same circumstances.

Gaseous spectral considerations are only important to the present problem if the absorptivity of the surface is a strong function of wavelength, which it appears not to be. Specifically, the spectral absorptivity of phenolic nylon ranges approximately between 1.0 and 0.8, of oxidized graphite between 1.0 and 0.9, and of zirconia between 0.9 and 0.8 for wavelengths between 0.34 and 0.74 microns at temperatures between 2300° and 3300° K (ref. 51).

at $y = 0$

$$\left.\begin{aligned} u &= 0 \\ v &= v_w \\ j &= j_w \\ \left(\partial c_f/\partial y\right)_w &= -\left(v_w/D_{f_w}\right)\left(1-c_{f_w}\right) \end{aligned}\right\} \quad (A14)$$

at $y = \delta$

$$\left.\begin{aligned} u &= u_s = Ux/R \\ v &= v_s = -\epsilon U(1 - x^2/2R^2) \\ p &= p_s = \rho_\infty U^2(1-\epsilon)(1-x^2/R^2) \\ j &= j_s = U^2/2 \\ c_f &= 0 \end{aligned}\right\} \quad (A15)$$

The Planck mean mass absorption coefficient for a mixture of air and foreign species is used in equation (A6) and is approximated by

$$K = K_{air}\left[1 + c_f(\alpha - 1)\right] \quad (A16)$$

as in reference 1.

## TRANSFORMATIONS

The continuity equation (A3) is eliminated if a stream function is adopted which satisfies it. Thus,

$$\frac{\partial \omega}{\partial y} = \rho u r^k , \qquad \frac{\partial \omega}{\partial x} = -H\rho v r^k \quad (A17)$$

Coordinates are transformed from $x$ and $y$ to $\zeta$ and $\eta$ as independent variables by the transformations

$$\zeta(x) = \int_o^x \rho_s \mu_s \left(\frac{r}{H}\right)^{2k} u_s \, dx \quad (A18)$$

$$\eta(x,y) = \frac{u_s}{\sqrt{2\zeta}} \left(\frac{r}{H}\right)^k \int_o^y H^k \rho \, dy \tag{A19}$$

The stream function is redefined such that

$$f(\zeta,\eta) = \omega/\sqrt{2\zeta} \tag{A20}$$

Thus from equations (A17) to (A20)

$$\frac{u}{u_s} = \frac{\partial f}{\partial \eta} \tag{A21}$$

Using the above transforms and the definitions

$$g = j/j_s \tag{A22}$$

$$\overline{T} = T/T_s \tag{A23}$$

$$\overline{K} = K/K_s \tag{A24}$$

$$\varphi = \rho\mu H^k/\rho_s\mu_s H_s{}^k \tag{A25}$$

equations (A4), (A6), and (A7) become (assumming that $\rho_s\mu_s$ is constant and similarity exists)

$$(\varphi f'')' + ff'' = \frac{1}{(k+1)} \left[(f')^2 - 2\frac{\rho_\infty}{\rho}(1-\epsilon)\right] \tag{A26}$$

$$\left(\frac{\varphi g'}{Pr}\right)' + fg' = -\left[\frac{4R\sigma T_s{}^4 K_s}{(k+1)U^3}\right] \overline{K} \left[\int_o^{t_s} \overline{T}^4(t) E_1(|t-\tau|)dt - 2\overline{T}^4 + \overline{T}_w{}^4 E_2(\tau)\right] \tag{A27}[2]$$

---

[2]For very optically thin shock layers (small R, U, or $p_s$), reabsorption in the gas is so slight that the method of evaluating the integral on the right side of equation (A27)(as described in ref. 1) breaks down. In that case the entire right side of equation (A27) may be replaced by

$$+\left[\frac{8R\sigma T_s{}^4 K_s}{(k+1)U^3}\right] \overline{T}^4 \overline{K}$$

and

$$\left(\frac{\varphi}{Sc}\, c_f'\right)' + f c_f' = 0 \qquad (A28)^3$$

respectively, where if it is assumed that $\rho = \rho(y)$

$$\tau = K_s \sqrt{\frac{\rho_s \mu_s R}{U(k+1)}} \int_o^{\eta} \frac{}{K}\, d\eta \qquad (A29)$$

The boundary conditions (A14) and (A15) transform to

at $\eta = 0$

$$\left.\begin{aligned} f &= f_w = -\rho_w v_w \sqrt{\frac{R}{\rho_s \mu_s U(k+1)}} \\ f' &= 0 \\ g &= g_w = \frac{2h_w}{U^2} \\ c_f' &= c_{f_w}' = \left(\frac{Sc}{\varphi}\right)_w f_w \left(1 - c_{f_w}\right) \end{aligned}\right\} \qquad (A30)$$

and at $\eta = \eta_s$

$$\left.\begin{aligned} f &= f_s = \rho_\infty \sqrt{\frac{RU}{\rho_s \mu_s (k+1)}} \\ f' &= f_s' = 1 \\ g &= g_s = 1 \\ c_f &= c_{f_s} = 0 \end{aligned}\right\} \qquad (A31)^4$$

---

[3]For want of better information, Sc was set equal to Pr in actual calculations involving the foreign species. A physical reasoning for this procedure may be thought of as follows. In general, the thermodynamic and transport properties used for the flow-field solutions are those of partially ionized and dissociated air. However, foreign species diffusion effects are treated as though the mixture were binary, a foreign species and air. The use of Schmidt number which varies like the Prandtl number then implies a constant Lewis number of unity. This binary approach is not too disagreeable even for atomic ionized air. In an analysis of a partially ionized diatomic gas (ref. 52), three species, atoms, atomic ions, and electrons were treated as a single species which diffuses as a unit with respect to molecules and the results were reasonable.

[4]The value of $\eta_s$ is actually determined where both $f_s$ and $f_s'$ are satisfied simultaneously.

## SHOCK STANDOFF DISTANCE AND HEAT TRANSFER

The shock standoff distance is

$$\delta = \sqrt{\frac{R\rho_s\mu_s}{U(k+1)}} \int_0^{\eta_s} \frac{d\eta}{\rho} \tag{A32}$$

The total net heat-transfer rate at the surface is the sum of the convective and radiative heating rates and is

$$q_T = -\left(\frac{\varphi}{Pr}\right)_w \frac{U^{5/2}}{2} \sqrt{\frac{\rho_s\mu_s(k+1)}{R}}\, g'(0) + \sigma T_s^4 \left[\bar{T}_w^4 - 2\int_0^{t_s} \bar{T}^4(t)E_2(t)dt\right] \tag{A33}^5$$

## SOLUTION OF THE EQUATIONS

The procedure for solving the set of integro-differential equations (A26), (A27), and (A28) subject to boundary conditions (A30) and (A31) is described in detail in reference 1. Briefly, it is an interative procedure initiated by the assumption of profiles of $\varphi$, $\varphi/Pr$, $\rho^{-1}$, and values of the right side of equations (A27) as functions of $\eta$. Equation (A26) is repeatedly integrated numerically by use of the Adams-Moulton predictor-corrector variable step integration scheme (ref. 53) until a value of $f''(0)$ is obtained for which the numerical solutions satisfy the first two of boundary conditions (A31). That solution of equation (A26) is then employed in solving equation (A27) for profiles of $g$ (enthalpy). New profiles of $\varphi$, $\varphi/Pr$, $\rho^{-1}$, and values of the right side of equation (A7) are calculated by use of the $g$ profiles and the entire process is repeated until convergence is obtained. The quantities $\varphi$, $\varphi/Pr$, $\rho^{-1}$, $\bar{T}$, and $\bar{K}$ as functions of enthalpy at constant pressure used in the computation were obtained from reference 54 and are based on the results of references 55, 48, and 28.

The computations were performed by use of the IBM 7094 digital computer. A solution at one flight condition required from 5 to 15 minutes of machine time.

---

[5]Again for very optically thin shock layers, the method of reference 1 for evaluating the integral on the right side of equation (A33) breaks down. In this case the term $-2\int_0^{t_s} \bar{T}^4(t)E_2(t)dt$ can be replaced by

$$-2K_s\sqrt{\frac{R\rho_s\mu_s}{U(k+1)}} \int_0^{\eta_s} \overline{\bar{T}^4\bar{K}}\, d\eta$$

## APPENDIX B

## BOUNDARY CONDITIONS BEHIND BOW SHOCK WAVE FOR VERY SMALL NOSE RADII OR REYNOLDS NUMBER

The outer boundary condition (A15) employed for the energy equation (A6) is

$$j_s = U^2/2 \tag{B1}$$

However, for nose radii small enough that a conductive heat flux exists just behind the shock, the boundary condition may be quite different from equation (B1) as follows.[1]

For simplicity, we consider only the normal portion of the shock wave and equate energy flux on each side of the shock thus,

$$\rho_\infty U \left(h_\infty + \frac{U^2}{2}\right) + \left(\frac{k}{c_p}\frac{dh}{dy}\right)_\infty = -\rho_s v_s \left(h_s + \frac{v_s^2}{2}\right) + \left(\frac{k}{c_p}\frac{dh}{dy}\right)_s \tag{B2}$$

where $y$ and $v$ are positive outward from the body. We employ the strong shock approximation

$$h_\infty \ll \frac{U_\infty^2}{2} \tag{B3}$$

and assume

$$\left(\frac{dh}{dy}\right)_\infty = 0 \tag{B4}$$

From mass continuity,

$$-v_s = \epsilon U \tag{B5}$$

By use of equations (B2) through (B5)

$$j_s = \frac{U^2}{2} - \frac{1}{\rho_\infty U}\left(\frac{k}{c_p}\frac{dh}{dy}\right)_s \tag{B6}$$

---

[1] A similar difficulty exists with the outer boundary conditions on the momentum equation because of vorticity behind the shock, as noted in reference 46. One way out of these difficulties is to integrate through the shock wave and use the free stream as boundary conditions, as presented in reference 56. Even at that, many uncertainties in the shock wave (e.g., thermal and chemical relaxation phenomena) remain at these high velocities.

So we see that $j_s$ is always less than $U^2/2$ by an amount that cannot be determined until the solution of the flow field behind the shock has been obtained and $(dh/dy)_s$ is known. The problem at once becomes one of iterating not only on the simultaneous differential equations, but on their boundary conditions as well.

We can estimate how much $j_s$ differs from $U^2/2$ by assuming

$$\frac{dh}{dy} = \frac{h_s - h_w}{\delta} \approx \frac{h_s}{\delta} \tag{B7}$$

Then $j_s$ becomes

$$j_s = \frac{U^2}{2} \frac{(1 + \epsilon^2\gamma)}{(1 + \gamma)} \tag{B8}$$

where

$$\gamma = \frac{1}{\rho_\infty U \left(\frac{\delta}{R}\right) R} \left(\frac{k}{c_p}\right)_s = \frac{Pr_s}{Re \left(\frac{\delta}{R}\right)} \tag{B9}$$

Since $\delta/R$ is not a strong function of $R$, $U$, or $p_s$ in the examples considered, $\gamma$ is inversely proportional to the Reynolds number and directly proportional to the Prandtl number behind the shock wave. If $\gamma \ll 1$, we have the usual boundary condition $j_s = U^2/2$. However, as $Re$ gets smaller, that is,

| if | then | |
|---|---|---|
| $\gamma \approx 1$ | $j_s \approx \frac{U^2}{4}$ | (B10) |
| $\gamma \gg 1$ | $j_s \approx \frac{U^2}{2}\left(\frac{1}{\gamma} + \epsilon^2\right)$ | |
| $\epsilon^2\gamma \gg 1$ | $j_s \approx \frac{U^2}{2}\epsilon^2$ | |

In the limit the approximation tells us that $j_s$ is much less than $U^2/2$.

For the moment, we adopt the point of view that $j_s$ was specified, and that the result of the corresponding solution might apply directly to a higher flight speed. That is, the true flight speed is larger than the assumed flight speed by the factor $\sqrt{(1 + \gamma)/(1 + \epsilon^2\gamma)}$. For the results in question, shown in figure 29, the factor varies from 1.0 to 1.2.

However, we cannot make direct application to the higher speed because we then violate another of boundary conditions (A15) in which the smaller value of $U$ was employed; namely, $\rho_s v_s = -\rho_\infty U$. For these reasons, the present low Reynolds number results are considered to be first approximations.

## REFERENCES


1. Howe, J. T., and Viegas J. R.: Solutions of the Ionized Radiating Shock Layer Including Reabsorption and Foreign Species Effects and Stagnation Region Heat Transfer. NASA TR R-159, 1963.

2. Lees, L.: Convective Heat Transfer With Mass Addition and Chemical Reactions. Presented at AGARD Combustion and Propulsion Colloquium, NATO, Palermo, Sicily, 1958 (GALCIT Pub. 451).

3. Lees, L.: Ablation in Hypersonic Flows. Paper presented at the Seventh Anglo-American Aeronautical Conference, New York, Oct. 5-7, 1959 (GALCIT Pub. 481).

4. Hayes, Wallace D.: Some Aspects of Hypersonic Flow. Ramo-Wooldridge Corp., Jan. 4, 1955.

5. Hoshizaki, H.: Heat Transfer in Planetary Atmospheres at Supersatellite Speeds. ARS paper 2173-61, ARS Jour., vol. 32, Oct. 1962, pp. 1544-51.

6. Cohen, N. B.: Boundary-Layer Similar Solutions and Correlation Equations for Laminar Heat-Transfer Distribution in Equilibrium Air at Velocities up to 41,000 ft/sec. NASA TR R-188, 1961.

7. Yoshikawa, K. K., and Chapman, D. R.: Radiative Heat Transfer and Absorption Behind a Hypersonic Normal Shock Wave. NASA TN D-1424, 1962.

8. Adams, Mac C.: Recent Advances in Ablation. ARS Jour., vol. 29, no. 9, Sept. 1959, pp. 625-632.

9. Georgiev, S., Hidalgo, H., and Adams, M. C.: On Ablation for the Recovery of Satellites. Res. Rep. 47, AVCO Res. Lab., March 1959.

10. Gross, J. J., Masson, D. J., and Gazley, C., Jr.: General Characteristics of Binary Boundary Layers With Application to Sublimation Cooling. Rand Rep. P-1371, 1958.

11. Stewart, J. D.: Transpiration Cooling: An Engineering Approach. General Electric Rep. MSVD-TIS-R 59SD338, May 1, 1959.

12. Swann, Robert T.: Effect of Thermal Radiation From a Hot Gas Layer on Heat of Ablation. Jour. Aero. Sci., vol. 28, no. 7, July 1961, pp. 582-583.

13. Swann, R. T., and Pittman, C. M.: Numerical Analysis of the Transient Response of Advanced Thermal Protection Systems for Atmosphere Entry. NASA TN D-1370, 1962.

14. Beckwith, I. E.: Similar Solutions for the Compressible Boundary Layer on a Yawed Cylinder With Transpiration Cooling. NACA TN 4345, 1958.

15. Lundell, J. H., Winovich, W., and Wakefield, R. M.: Simulation of Convective and Radiative Entry Heating. Arthur M. Krill, ed., Advances in Hypervelocity Techniques Proc. Second Symposium on Hypervelocity Techniques. Plenum Press, New York, 1962, pp. 729-748.

16. Scala, S. M.: The Ablation of Graphite in Dissociated Air, Part I, Theory. IAS paper 62-154, 1962 (also General Electric Co. Missile and Space Division, R 62SD72, Sept. 1962).

17. Hartnett, J. P., and Eckert, E. R. G.: Mass Transfer Cooling With Combustion in a Laminar Boundary Layer. Heat Transfer and Fluid Mechanics Institute, Univ. of Calif., Berkeley, 1958, Stanford U. Press, Stanford, Calif., 1958, pp. 54-68.

18. Cohen, C. B., Bromberg, R., and Lipkis, R. P.: Boundary Layers With Chemical Reactions Due to Mass Addition. Jet Propulsion, vol. 28, no. 10, Oct. 1958, pp. 659-668.

19. Vojvodich, N. S., and Pope, R. B.: An Investigation of the Effect of Gas Composition on the Ablation Behavior of a Charring Material. Paper for ARS and MIT Conference on Physics of Entry Into Planetary Atmospheres (AIAA), Cambridge, Mass., Aug. 1963.

20. Chung, P. M.: Shielding Stagnation Surfaces of Finite Catalytic Activity by Air Injection in Hypersonic Flight. NASA TN D-27, 1959.

21. Lees, Lester: Similarity Parameters for Surface Melting of a Blunt Nosed Body in a High Velocity Gas Stream. ARS Jour., vol. 29, no. 5, May 1959, pp. 345-354.

22. Bethe, Hans A., and Adams, Mac C.: A Theory for the Ablation of Glassy Materials. JAS, vol. 26, no. 6, June 1959, pp. 321-328 and p. 350.

23. Allen, H. J., Seiff, A., and Winovich, W.: Aerodynamic Heating of Conical Entry Vehicles at Speeds in Excess of Earth Parabolic Speed. NASA TR R-185, 1963.

24. Allen, H. J., and James, N.: Prospects for Obtaining Aerodynamic Heating Results From Analysis of Meteor Flight Data. NASA TN D-2069, 1964.

25. Howe, John T., Viegas, John F., and Sheaffer, Yvonne S.: Study of the Nonequilibrium Flow Field Behind Normal Shock Waves in Carbon Dioxide. NASA TN D-1885, 1963.

26. Chung, P. M.: Hypersonic Viscous Shock Layer of Nonequilibrium Dissociating Gas. NASA TR R-109, 1961.

27. Page, W. A., and Arnold, J. O.: Shock Layer Radiation of Blunt Bodies at Reentry Velocities. NASA TR R-193, 1964.

28. Kivel, B., and Bailey, K.: Tables of Radiation From High Temperature Air. Res. Rep. 21, AVCO Res. Lab., Dec. 1957.

29. Wick, Bradford H.: Radiative Heating of Vehicles Entering the Earth's Atmosphere. Paper presented to the Fluid Mechanics Panel of AGARD, Brussels, 1962.

30. Craig, Roger A., and Davy, William C.: Thermal Radiation From Ablation Products Injected Into a Hypersonic Shock Layer. NASA TN D-1978, 1963.

31. Rose, P. H., and Stark, W. I.: Stagnation Point Heat-Transfer Measurements in Dissociated Air. Jour. Aero. Sci., vol. 25, no. 2, Feb. 1958, pp. 86-97.

32. Stankevics, J. O., and Rose, P. H.: Stagnation Point Heat Transfer in Partially Ionized Air. IAS Paper 63-61, 1963.

33. Compton, Dale L., and Chapman, Gary T.: Two New Free-Flight Methods for Obtaining Convective Heat-Transfer Data. Paper presented at AIAA Testing Conference, March 1964.

34. Offenharty, E., Weisblatt, H., and Flagg, R. F.: Stagnation Point Heat Transfer Measurements at Supersatellite Speeds. Jour. Roy. Aero. Soc., vol. 66, no. 613, Jan. 1962, p. 53.

35. Fay, James A.: Hypersonic Heat Transfer in the Air Laminar Boundary Layer. Paper presented at Hypersonic Specialists Conference, AGARD, Brussels, Belgium, Apr. 3-6, 1962.

36. Pallone, A., and Van Tassell, W.: Stagnation Point Heat Transfer for Air in the Ionization Regime. ARS Jour., vol. 32, no. 3, March 1962, pp. 436-7.

37. Ferri, Antonio, Zakkay, Victor, and Ting, Lu: Blunt-Body Heat Transfer at Hypersonic Speed and Low Reynolds Numbers. Jour. Aero. Sci., vol. 28, no. 12, Dec. 1961, pp. 962-971 and p. 991.

38. Ferri, Antonio, and Zakkay, Victor: Measurements of Stagnation Point Heat Transfer at Low Reynolds Numbers. Jour. Aero. Sci., vol. 29, no. 2, July 1962, pp. 847-850.

39. Probstein, R. F.: Shock Wave and Flow Field Development in Hypersonic Reentry. Paper presented at the ARS Semiannual Meeting, Los Angeles, May 9-12, 1960, ARS Preprint 1110-60.

40. Cheng, H. K.: Hypersonic Shock-Layer Theory of the Stagnation Region at Low Reynolds Numbers. Proc. of the 1961 Heat Trans. and Fluid Mech. Inst. Stanford University Press, Stanford, Calif., 1961, pp. 161-175.

41. Hayes, Wallace D., and Probstein, Ronald F.: Hypersonic Flow Theory. Academic Press, Inc., New York, 1959, p. 372.

42. Hickman, R. S., and Giedt, W. H.: Heat Transfer to a Hemisphere-Cylinder at Low Reynolds Numbers. AIAA Jour., vol. 1, no. 3, March 1963, pp. 665-672.

43. Tong, Henry, and Giedt, W. H.: Supersonic Stagnation Point Heat Transfer at Low Reynolds Numbers. AIAA Jour., vol. 2, 1964, pp. 185-186.

44. Van Dyke, Milton: Second-Order Compressible Boundary Layer Theory With Application to Blunt Bodies in Hypersonic Flow. Hypersonic Flow Res., Academic Press, Inc., New York, 1962, pp. 37-76.

45. Van Dyke, Milton: A Review and Extension of Second-Order Hypersonic Boundary-Layer Theory. Rarefied Gas Dynamics, vol. 2, Academic Press, Inc., New York, 1963, pp. 212-227.

46. Hoshizaki, H.: Shock Generated Vorticity Effects at Low Reynolds Numbers. Tech. Rep. LMSD-48381, Missile and Space Division, 1959.

47. Emmons H. W., and Leigh , D.: Tabulation of the Blasius Function with Blowing and Suction. Combustion Aerodynamics Lab., Interim Tech. Rep. 9, Harvard Univ., Nov. 1953.

48. Hansen, C. Frederick: Approximations for the Thermodynamic and Transport Properties of High-Temperature Air. NASA TR R-50, 1959.

49. Butler, James N., and Brokaw, Richard S.: Thermal Conductivity of Gas Mixtures in Chemical Equilibrium. Jour. Chem. Phys., vol. 26, no. 6, June 1957, pp. 1636-1643.

50. Martin, E. Dale: Boundary Shock Waves and Boundary Shock Structure. Prospective NASA Report.

51. Wilson, G. R.: Hemispherical Spectral Emittance of Ablation Chars, Carbon and Zirconia to 6000° F. Paper presented at Symposium on Thermal Radiation of Solids, San Francisco, Calif., Mar. 1964.

52. Fay, J. A., and Kemp, N. H.: Theory of Stagnation Point Heat Transfer in a Partially Ionized Diatomic Gas. AIAA Jour., vol. 1, no. 12, Dec. 1963, pp. 2741-2751.

53. Hildebrand, F. B.: Introduction to Numerical Analysis. McGraw-Hill Book Co., New York, 1956.

54. Viegas, J. R., and Howe, J. T.: Thermodynamic and Transport Property Correlation Formulas for Equilibrium Air From 1,000° K to 15,000° K. NASA TN D-1429, 1962.

55. Moeckel, W. E., and Weston, K. D.: Composition and Thermodynamic Properties of Air in Chemical Equilibrium. NACA TN 4265, 1958.

56. Probstein, R. F., and Kemp, N. H.: Viscous Aerodynamic Characteristics in Hypersonic Rarefied Gas Flow. Jour. Aero/Space Sci., vol. 27, March 1960, pp. 174-192.

57. Kratsch, K. M., Hearne, L. F., and McChesney, H. R.: Thermal Performance of Heat Shield Composites During Planetary Entry. Presented at AIAA-NASA National Meeting, Palo Alto, Calif., 1963.

TABLE I.- CONDITIONS FOR POINTS SHOWN IN

FIGURES 3 AND 4

| Group | Point | $p_s$, atm | $\bar{U}$ | R, ft | $-f_w$ | Comments |
|---|---|---|---|---|---|---|
| 1 | 1 | 1.0 | 4.1 | 0.01 | 0.1 | |
| | 2 | 1.0 | 4.1 | 1.0 | .1 | |
| | 3 | 1.0 | 5.0 | 1.0 | .2 | |
| 2 | 4 | 1.0 | 5.0 | 1.0 | .4 | |
| | 5 | 1.0 | 5.0 | 1.0 | .45 | |
| | 6 | 1.0 | 5.0 | .1 | .5 | |
| | 7 | 1.0 | 5.0 | .25 | .5 | |
| | 8 | 1.0 | 5.0 | .5 | .5 | |
| | 9 | 1.0 | 5.0 | 1.0 | .5 | |
| | 10 | 1.0 | 5.0 | 2.0 | .5 | |
| | 11 | .1 | 5.0 | 5.0 | .5 | |
| 3 | 12 | 10.0 | 4.0 | .1 | .5 | |
| | 13 | 10.0 | 4.0 | .25 | .5 | |
| | 14 | 1.0 | 4.0 | 1.0 | .5 | |
| | 15 | 1.0 | 3.0 | 1.0 | .5 | |
| | 16 | 1.0 | 5.0 | 1.0 | .75 | |
| 4 | 17 | 1.0 | 5.0 | .1 | 1.0 | } appear as one point |
| | 18 | 1.0 | 5.0 | .25 | 1.0 | } on figures 3 and 4 |
| | 19 | 1.0 | 5.0 | .5 | 1.0 | |
| | 20 | 1.0 | 5.0 | 1.0 | 1.0 | |
| | 21 | .1 | 5.0 | 5.0 | 1.0 | |
| 5 | 22 | 1.0 | 5.0 | 1.0 | 1.25 | |
| | 23 | 1.0 | 4.1 | .01 | 1.0 | |
| | 24 | 1.0 | 4.1 | 1.0 | 1.0 | |
| | 25 | 10.0 | 4.0 | .1 | 1.0 | } appear as one point |
| | 26 | 10.0 | 4.0 | .25 | 1.0 | } on figures 3 and 4 |
| | 27 | 1.0 | 4.0 | 1.0 | 1.0 | |
| 6 | 28 | 1.0 | 3.0 | 1.0 | 1.0 | |
| | 29 | 1.0 | 5.0 | .1 | 1.5 | } appear as one point |
| | 30 | 1.0 | 5.0 | .25 | 1.5 | } on figures 3 and 4 |
| | 31 | 1.0 | 5.0 | .5 | 1.5 | } appear as one point |
| | 32 | 1.0 | 5.0 | 1.0 | 1.5 | } on figures 3 and 4 |
| | 33 | .1 | 5.0 | 5.0 | 1.5 | |
| 7 | 34 | 10.0 | 4.0 | .25 | 1.5 | } appear as one point |
| | 35 | 1.0 | 4.0 | 1.0 | 1.5 | } on figures 3 and 4 |
| 8 | 36 | 1.0 | 5.0 | 1.0 | 2.0 | |

TABLE II.- CONDITIONS FOR POINTS SHOWN

IN FIGURE 5

| Point | $p_s$, atm | $\bar{U}$ | R, ft | $-f_w$ |
|---|---|---|---|---|
| 1 | 1 | 4.1 | 0.01 | 0.1 |
| 2 | 1 | 4.1 | 1 | .1 |
| 3 | 1 | 5 | 1 | .2 |
| 4 | 1 | 5 | .1 | .5 |
| 5 | 1 | 5 | 1 | .4 |
| 6 | 1 | 5 | .25 | .5 |
| 7 | .1 | 5 | 5 | .5 |
| 8 | 1 | 5 | .5 | .5 |
| 9 | 1 | 5 | 1 | .45 |
| 10 | 1 | 5 | 1 | .5 |
| 11 | 1 | 5 | 2 | .5 |
| 12 | 10 | 4 | .1 | .5 |
| 13 | 1 | 4 | 1 | .5 |
| 14 | 1 | 5 | .1 | 1 |
| 15 | 1 | 5 | 1 | .75 |
| 16 | 10 | 4 | .25 | .5 |
| 17 | 1 | 3 | 1 | .5 |
| 18 | 1 | 5 | .25 | 1 |
| 19 | 1 | 4 | .01 | 1 |
| 20 | .1 | 5 | 5 | 1 |
| 21 | 1 | 5 | .5 | 1 |
| 22 | 1 | 5 | 1 | 1 |
| 23 | 1 | 5 | .1 | 1.5 |
| 24 | 1 | 5 | .25 | 1.5 |
| 25 | .1 | 5 | 5 | 1.5 |
| 26 | 1 | 5 | 1 | 1.25 |
| 27 | 1 | 5 | .5 | 1.5 |
| 28 | 10 | 4 | .1 | 1 |
| 29 | 1 | 4.1 | 1 | 1 |
| 30 | 1 | 4 | 1 | 1 |
| 31 | 1 | 5 | 1 | 1.5 |
| 32 | 10 | 4 | .25 | 1 |
| 33 | 1 | 3 | 1 | 1 |
| 34 | 1 | 5 | 1 | 2 |
| 35 | 1 | 4 | 1 | 1.5 |
| 36 | 10 | 4 | .25 | 1.5 |

TABLE III.- PROPERTIES OF ABLATING SURFACES[1]

| Material | $h_a$, $ft^2/sec^2$ | $T_w$, $^oK$ | $\epsilon_w$ | $\alpha_w$ |
|---|---|---|---|---|
| Teflon[2] | $2.38 \times 10^7$ (8) | 1000 | 1 and 0.5 | 1 and 0.5 |
| Phenolic nylon | $3.755 \times 10^7$ (8) | 3700 (57) | 0.6 (57) | 0.6 (57) |

[1]Values in the table are estimates made from information in the references shown in parentheses.

[2]The temperature shown for Teflon is higher than the 800° F (or 700° K) given by reference 8. However, it is of no consequence because reradiation from the higher temperature is still negligible. It should be noted that in applying our $\psi$ results to Teflon, we have not made any allowance for the presence of a finite asymptote (see footnote, p. 10). If indeed a finite asymptote does exist at hypervelocity, we must consider our Teflon results to apply instead to a material which has the properties shown above but which does not have a finite $\psi$ asymptote.

TABLE IV.- SCALING FOREIGN SPECIES EXAMPLES

| Figure | $U \times 10^{-4}$, ft/sec | $p_s$, atm | $-f_w$ | $\frac{\dot{m}}{\rho_\infty U}$ | R, ft | Re |
|---|---|---|---|---|---|---|
| 18 | 4.1 | 1 | 1.0 | 0.5 | 0.01 | $1.14 \times 10^2$ |
| 19 | 4.1 | 1 | .1 | .05 | .01 | $1.14 \times 10^2$ |
| 20 | 4.1 | 1 | 1.0 | .05 | 1.0 | $1.14 \times 10^4$ |
| 21 | 4.1 | 1 | .1 | .005 | 1.0 | $1.14 \times 10^4$ |
| 22 | 3 | 1 | .3 | .05 | .063 | $1.19 \times 10^3$ |
| 23 | 4.1 | 10 | .3 | .05 | .011 | $1.05 \times 10^3$ |
| 24 | 4.1 | 1 | .3 | .05 | .1 | $1.14 \times 10^3$ |
| 25 | 5 | 1 | .3 | .05 | .074 | $1.26 \times 10^3$ |



NASA-Langley, 1964 A-940